

7-2023

## **A Data-Driven Method for Damage Detection in an Open Deck Steel Truss Railroad Bridge Under the Moving Train Load**

Mahesh Pokhrel  
*The University of Texas Rio Grande Valley*

Follow this and additional works at: <https://scholarworks.utrgv.edu/etd>



Part of the [Transportation Engineering Commons](#)

---

### **Recommended Citation**

Pokhrel, Mahesh, "A Data-Driven Method for Damage Detection in an Open Deck Steel Truss Railroad Bridge Under the Moving Train Load" (2023). *Theses and Dissertations - UTRGV*. 1277.  
<https://scholarworks.utrgv.edu/etd/1277>

This Thesis is brought to you for free and open access by ScholarWorks @ UTRGV. It has been accepted for inclusion in Theses and Dissertations - UTRGV by an authorized administrator of ScholarWorks @ UTRGV. For more information, please contact [justin.white@utrgv.edu](mailto:justin.white@utrgv.edu), [william.flores01@utrgv.edu](mailto:william.flores01@utrgv.edu).

A DATA-DRIVEN METHOD FOR DAMAGE DETECTION IN  
AN OPEN DECK STEEL TRUSS RAILROAD BRIDGE  
UNDER THE MOVING TRAIN LOAD

A Thesis  
by  
MAHESH POKHREL

Submitted in Partial Fulfillment of the  
Requirements for the Degree of  
MASTER OF SCIENCE

Major Subject: Civil Engineering

The University of Texas Rio Grande Valley

July 2023



A DATA-DRIVEN METHOD FOR DAMAGE DETECTION IN  
AN OPEN DECK STEEL TRUSS RAILROAD BRIDGE  
UNDER THE MOVING TRAIN LOAD

A Thesis  
by  
MAHESH POKHREL

COMMITTEE MEMBERS

Dr. Mohsen Amjadian  
Chair of Committee

Dr. Philip Park  
Committee Member

Dr. Mohamadossein Noruzoliaee  
Committee Member

July 2023



Copyright 2023 Mahesh Pokhrel

All Rights Reserved



## ABSTRACT

Pokhrel, Mahesh, A Data-Driven Method for Damage Detection in an Open Deck Steel Truss Railroad Bridge under the Moving Train Load. Master of Science (MS), July, 2023, 95 pp., 7 tables, 44 figures, references, 44 titles.

Open-Deck (OD) steel truss railroad bridges are one of the most common types of railroad bridges in the United States. They are, however, significantly vulnerable to the dynamic effects of moving train load. In the long run, these dynamic effects cause fatigue damage to the structural members. The damage in most of the railroad bridges are monitored by visual inspections which are sometimes unreliable and inconsistent due to human error. This study explores the identification and classification of damage to an open deck railroad bridge from both time-domain (statistical features) and time-frequency domain features (Hilbert-Huang Transform) extracted through acceleration response using Machine Learning Classifier in MATLAB R2022a. A 3D finite element model of the bridge was created in SAP2000 and validated with the field-testing data. The changes in acceleration time-history responses obtained under the different damage cases are utilized to detect damage using two Machine Learning Classifiers: Support Vector Machine (SVM) and K-Nearest Neighbor (KNN) algorithms. The extracted features are used to train and cross validate the algorithm and indicated high level of precision (more than 95%) in identifying and classifying the damage in the bridge and more than 85% in identifying defect in the rail.



## DEDICATION

The completion of my Master of Science studies would not have been possible without the love and support of my family. My mother, Ramma Pokhrel, my father, Megha Raj Sharma, my wife, Shova Subedi, and my son, Sameep Pokhrel, wholeheartedly inspired, motivated, and supported me by all means to accomplish this degree. Thank you for your love and patience.



## ACKNOWLEDGMENTS

The satisfaction and excitement on the successful completion of any important task would be incomplete without the mention of the people who made it possible, whose constant guidance and encouragement crowned my effort with success.

I will always be grateful to Dr. Mohsen Amjadian, chair of my thesis committee, for all his mentoring, scholarly advice, and critical discussions. From research design, and data processing to manuscript editing, he continuously encouraged me to complete this process through his infinite patience and guidance. His constant scrutiny and suggestions supported me in the critical stages. My sincere thanks and deep gratitude go to my thesis committee members: Dr. Philip Park, and Dr. Mohamadossein Noruzoliaee. Their advice, input, and comments on my thesis helped me to ensure the quality of my intellectual work.

I am also grateful to the professors Dr. Jungseok Ho, Dr. Jong-Min Kim, Dr. Mohamed Abdel Raheem, Dr. Thang Pham, Dr. Fatemeh (Noosheen) Nazari, Dr. Yooseob Song and Dr. Thuy Vu for their excellent course works and cooperations during thesis work.

I would like to gratefully acknowledge the support and assistance provided by The University of Texas Rio Grande Valley (UTRGV) in terms of the Presidential Research Fellowship Award. Also, I would like to thank my colleagues and friends at the University of Texas Rio Grande Valley who helped me directly and indirectly by providing information and documents for my research.



## TABLE OF CONTENTS

	Page
ABSTRACT.....	iii
DEDICATION.....	iv
ACKNOWLEDGMENTS .....	v
TABLE OF CONTENTS.....	vi
LIST OF TABLES.....	ix
LIST OF FIGURES .....	x
CHAPTER I. INTRODUCTION.....	1
1.1. Introduction.....	1
1.2. Types of Railroad Bridges .....	1
1.3. Components of Railroad Bridges.....	3
1.4. Railroad Bridges in the U.S. ....	6
1.5. Damage detection in railroad bridges .....	7
1.6. Objectives and Scope of the Work.....	8
CHAPTER II. LITERATURE REVIEW .....	10
2.1. Damage to Railroad Bridges.....	10
2.2. Effects of Wheel-Rail Contact.....	17
2.3. Structural Health Monitoring of Railroad Bridges .....	18

2.4. Machine Learning Classification .....	19
2.5. Limitations of the Previous Research .....	21
<b>CHAPTER III. THEORY OF VIBRATION OF A SIMPLY SUPPORTED BEAM SUBJECTED TO MOVING LOADS .....</b>	<b>23</b>
3.1. Mathematical Formulation of moving load .....	23
3.1.1. Effect of Single Axle Load .....	23
3.1.2. Impact Factor for Midpoint Displacement.....	29
3.1.3. Effects of Series of Moving Loads .....	31
3.1.4. Resonance Conditions.....	36
3.1.5. Condition of Cancellation.....	37
3.2 Validation of the Moving Load Model in SAP2000.....	38
3.2.1. Single Axle Load .....	38
3.2.2 Double Axle Load.....	41
<b>CHAPTER IV. FINITE ELEMENT MODELING OF A RAILROAD BRIDGE.....</b>	<b>45</b>
4.1 Devon Railroad Bridge .....	45
4.2. Train Loading.....	47
4.3. Finite Element Model in SAP2000 .....	48
4.4. Model Validation .....	50
4.5. Natural Frequencies and Mode Shapes.....	51
4.6. Transient Time History Analysis .....	52
4.6.1. Sensitivity Analysis: Time Step .....	52
4.6.2. Sensitivity Analysis: Damping Ratio .....	53
4.7. Resonance Speed .....	54

CHAPTER V. DAMAGE QUANTIFICATION .....	56
5.1. Damage to the Stringer-to-Girder Joints.....	56
5.2. Defect in the Rail .....	60
5.3. Vibration Features.....	62
5.3.1. Time Domain Features .....	62
5.3.2. Time-Frequency Domain Features: Hilbert-Huang Transform.....	64
5.3.3. Feature Scaling (Normalization) .....	67
CHAPTER VI. DAMAGE CLASSIFICATION .....	70
6.1. Machine Learning Classifiers .....	70
6.1.1. Support Vector Machine (SVM) .....	70
6.1.2. K-Nearest Neighbor (KNN) .....	74
6.2. Damage Classification .....	75
6.2.1. Damage in the Bridge Deck without Rail Defect.....	76
6.2.2. Damage in the Bridge Deck with Rail Defect.....	80
6.2.3. Combination of damages in Bridge and Rail .....	83
CHAPTER VII. CONCLUSIONS.....	86
REFERENCES .....	88
APPENDIX.....	92
BIOGRAPHICAL SKETCH .....	95



## LIST OF TABLES

	Page
Table 4.1: Axial and Bending members in the Devon railroad bridge. ....	50
Table 4.2: Natural frequencies of different modes from FE model and field study .....	50
Table 4.3: Damping Ratio for different Modes of the Bridge .....	54
Table 5.1: Statistical Features in the Time Domain used for the extraction of features. ....	63
Table 6.1: Evaluation metrics for ML classifiers used in the data-analytic study. ....	79
Table 6.2: Evaluation metrics for ML classifiers used in the data-analytic study. ....	82
Table 6.3: Evaluation metrics for ML classifiers used in the data-analytic study. ....	85



## LIST OF FIGURES

	Page
Figure 1.1 Some types of railroad bridges, (a) Through Truss Bridge, (b) Deck Truss Bridge .....	2
Figure 1.2 Types of railroad bridges, (a) Through Plate Girder Bridge, (b) Deck Plate Girder Bridge (Lindamood et al., 2003).....	3
Figure 1.3 Open deck railroad bridge (Lindamood et al., 2003) .....	4
Figure 1.4 (a) Common components of railroad structure (b) Rail details.....	6
Figure 1.5 Union Pacific train derailment due to broken rail on a Tempe, Ariz., bridge in July 2020 (source: FRA Factual Railroad Accident Report HQ-2020-1390 and Article by Johnny Diaz on The New York Times dated July 29, 2020).....	8
Figure 3.1 Simply supported bridge subjected to a constant single axle moving load.....	23
Figure 3.2 Simply supported railroad bridge subject to (a) series of moving loads (b) actual train loads .....	31
Figure 3.3 Simply supported bridge subjected to a constant single moving load.....	38
Figure 3.4 Vertical displacement of simply supported beam subjected to a moving load .....	39
Figure 3.5 Vertical displacement and acceleration of Simply supported beam subjected to a moving load at different speeds .....	40
Figure 3.6 Maximum absolute vertical acceleration of Simply supported beam at different speeds .....	40
Figure 3.7 Maximum absolute vertical acceleration of Simply supported beam at different speeds .....	40

Figure 3.8 Simply supported bridge subjected to number of moving loads .....	41
Figure 3.9 Vertical displacement plot of Simply supported Railroad bridge subjected to train load.....	43
Figure 3.10 Vertical acceleration plot of Simply supported Railroad bridge subjected to train load,.....	43
Figure 3.11 Midpoint response of Simply supported Railroad bridge subjected to a train load at resonance and cancellation speeds in SAP 2000 .....	44
Figure 4.1 Photograph of Devon railroad bridge, Milford, Connecticut. (Malla et al., 2017) .....	46
Figure 4.2 Arrangement of principle members of Devon bridge (Baniya et al., 2015).....	46
Figure 4.3 Top Chord plan (Baniya et al., 2015).....	47
Figure 4.4 Bottom chord plan (Baniya et al., 2015) .....	47
Figure 4.5 Configuration of loading from Amtrak Acela Train .....	48
Figure 4.6 3D model of Amtrak Acela train and axle loads in SAP 2000.....	48
Figure 4.7 3D model of Devon Steel truss bridge in SAP 2000.....	49
Figure 4.8 Mode shapes of the bridge resulted from the FE model.....	52
Figure 4.9 Sensitivity analysis for optimum time step .....	53
Figure 4.10 Sensitivity analysis for damping ratio .....	53
Figure 4.11 Midspan vertical deflection and acceleration vs moving speed of Amtrak Acela Train.....	55
Figure 5.1 example of Stringer-to-Girder joint with possibility of cracks (Rageh, 2020).....	56
Figure 5.2 Details of a Joint including fatigue cracks(Rageh et al., 2020).....	57
Figure 5.3 Change of rotational stiffness with the progress of crack in the Stringer-to-Girder joint (Rageh et al., 2020).....	58

Figure 5.4 Devon railroad bridge elevation and plan with location of sensors and damage .....	59
Figure 5.5 Example of a broken rail .....	60
Figure 5.6 Modeling of a broken rail in the FE model. ....	61
Figure 5.7 Sensitivity Analysis for length of Crack in rail with the variation of displacement and acceleration at joint 1663. ....	61
Figure 5.8 Joint 1663 in the stringer below the edge of gap in the rail (broken rail) .....	62
Figure 5.9 Hilbert spectral analysis of the acceleration signal recorded by S2 for train speed of 15m/sec speed a) healthy rail healthy bridge acceleration b) healthy rail damaged bridge acceleration c) Healthy rail and healthy bridge Hilbert spectrum d) healthy rail damaged bridge Hilbert spectrum e) Rail defect highly damaged bridge acceleration f) Rail defect highly damaged bridge Hilbert spectrum .....	66
Figure 5.10 Energy and Instantaneous phase of recorded acceleration signals for S2 sensor location in the healthy rail and bridge compared to highly damaged bridge at 15 m/sec speed .....	69
Figure 6.1. Graphical representation of SVM classification with optimal and marginal hyperplanes.....	70
Figure 6. 2 Scatter plot of Energy vs different features (Healthy Rail).....	77
Figure 6. 3 Confusion matrix for SVM and KNN algorithms .....	78
Figure 6. 4 Scatter plot of Energy vs different features (Damaged Rail) .....	81
Figure 6. 5 Confusion matrix for SVM and KNN algorithms (Rail defect).....	82
Figure 6. 6 Scatter plot of Energy vs different features (Damaged vs Undamaged Rail & Bridge).....	84
Figure 6. 7 Confusion matrix for SVM and KNN algorithms (Damaged vs Undamaged Rail)...	85



## CHAPTER I

### INTRODUCTION

#### **1.1. Introduction**

Railroads are energy-efficient and cost-effective transportation modes for freight and people. The railroad structures have advanced significantly in recent years. Although there is not any specified material for railroad bridges, steel bridges are more widespread because of their easy installation and maintenance as well as replacement. Different materials used for the construction of railroad bridges have their own fits.

#### **1.2. Types of Railroad Bridges**

Simple-span bridges are the most common types of bridges for railroad alignment. More common types of railroad bridges and materials for different span lengths are described here.

For shorter spans up to 16 ft in length, Timber stringers, Concrete slabs and Rolled steel beams are used. Likewise, up to 32 ft in length; Conventional and prestressed concrete box girders and beams and Rolled steel beams are used. Similarly, up to 50 ft length of the bridge; prestressed concrete box girders and beams, rolled steel beams, deck, and through girders are used. For medium Span bridges, from 80 ft to 125 ft, prestressed concrete beams, and Deck and

through plate girders are used. For Longer Spans of more than 125 ft in length, through and deck trusses are used (Sorgenfrei & Marianos, 2000).

**Truss Bridges:** These bridges are the most common railroad bridges due to their efficiency and workability. Steel trusses are feasible for spans over 150 to 180 feet. Trusses are normally comprised of bottom and top chords connected by diagonal and vertical hangers. These parts are connected to form a bridge with the help of a bolt or rivet. Based on the type of connection of different parts and the position of the track, Truss railroad bridges can be categorized into three types.

**Through Truss Bridges:** The rail runs between the trusses and the members of the trusses are located above and below the track level. In this type of bridge, normally there are cross-bracings above and below the train.

**Deck Truss Bridges:** In these types of bridges, the level of rail is located at the top of the truss. All the bracings and superstructure are positioned below the track.

**Suspended Deck Truss Bridges:** The level of the rail is located on top of the truss, and the truss structure is supported by the truss at the top chord.

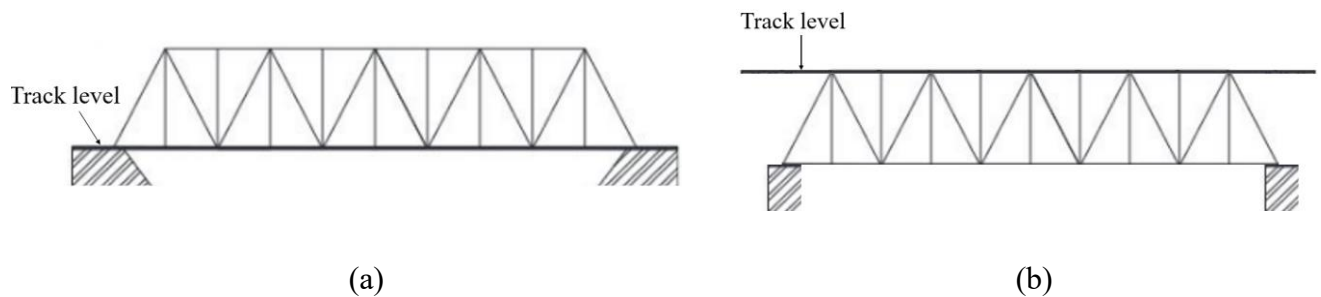


Figure 1.1 Some types of railroad bridges, (a) Through Truss Bridge, (b) Deck Truss Bridge

**Plate Girder Bridges:** One of the simplest type of bridges are the simple beam or girder railroad bridge. Two typical plate girder railroad bridges are (Kim & Spencer, 2015).

Through Plate Girder Bridge: The bridge consists of a girder with a track resting on the floor level. Normally these types of bridges have ties resting directly on the stringer. Through girder bridges are used to cross an obstacle when there is a concern of clearance below the bridge such as above the highway or crossing.

Deck Plate Girder Bridge: It consists of two girder plates with composite cross sections and girders are located under the track level. An additional floor is not required to support the rail, so these types of bridges are more cost-effective than through-plate girder bridges. These bridges are used when the vertical clearances below the track system are not a concern.

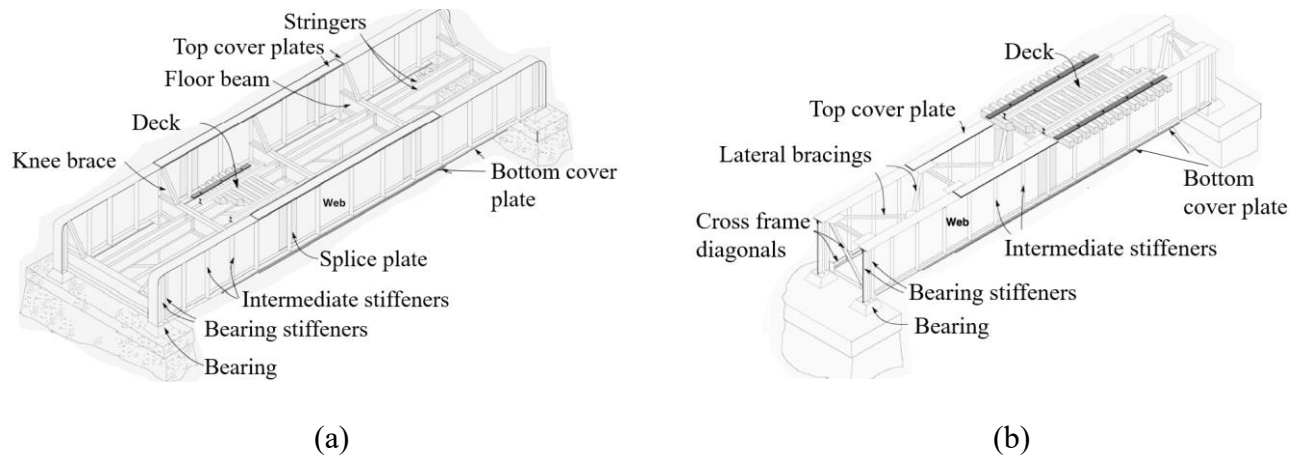


Figure 1.2 Types of railroad bridges, (a) Through Plate Girder Bridge, (b) Deck Plate Girder Bridge (Lindamood et al., 2003)

### 1.3. Components of Railroad Bridges

Railroad bridges are comprised of the structure, rails, ties or sleepers, and ballast. The rails are normally fixed to transverse sleepers which are set in a bed of crushed stone ballast. The bridges with the whole set of these components are called ballasted deck bridges. In some situations, sleepers and ballasts are not found in their position, but the rails are directly fastened

to the bridge deck, called open deck bridges. The ballasted deck is widely used in freight and regular-speed passenger routes, while the open deck is more common for high-speed routes. A ballasted deck provides a better riding track.

This study focuses on the Open-Deck (OD) bridge which has lesser dead loads and lower maintenance cost however sensitive to vibrations and causes rough riding and damage to the key structural members.

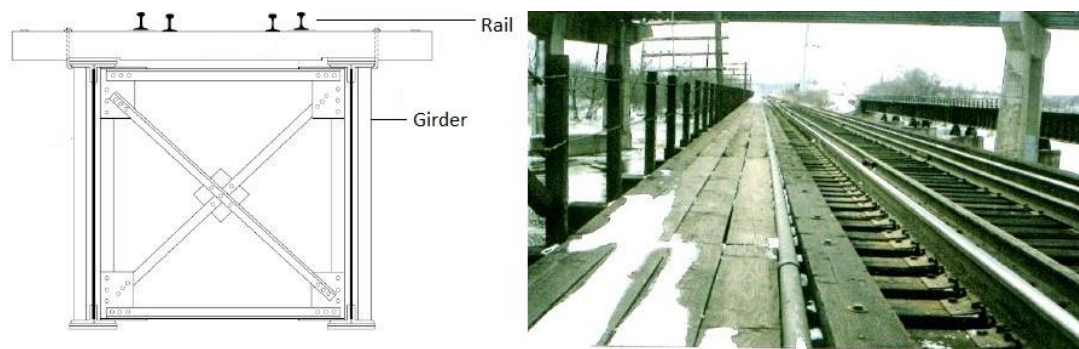


Figure 1.3 Open deck railroad bridge (Lindamood et al., 2003)

**Rail:** Rail is the longitudinal element of steel material that directs the wheel continuously and uniformly throughout the length. It also provides a smooth riding surface and accommodates the wheel loads to distribute over the sleepers and further down to the bridge deck. A steel rail has an I-section with a flat bottom as shown in figure 4 below.

Broken rails are a primary cause of train derailments resulting from track infrastructure faults. They can have severe effects on the service of rails in the U.S., and the large impact forces intensified during the passage of train at high speeds which causes a consequent rupture to rail and endanger running safety.

**Fasteners:** Fasteners connect the rails with the sleepers and resist the moments of the rails due to different loads from the wheel and temperature change. The selection of type of fastener depends on the geometry of the rail and type of sleeper.

**Rail Pad or Plate:** A rail pad is installed between the sleeper and the rail. The rail pads provide insulation to electricity from the rails and protect the sleepers from wear and tear.

**Sleepers or Ties:** Sleepers or Ties are the beams that span across the two rails to connect and tie them in position. The functions of sleepers are to receive the loads from the rail and distribute them over the ballast, hold the fasteners, and restrain the rail movement through the anchorage. Sleepers also provide a tilt to the rails to help develop proper wheel-rail contact and works as an electrical insulator between two rails. The ideal spacing between the sleepers is 0.6m.

**Ballast:** Ballast is the layer of crushed hard stone which provides support to the sleepers. The ballast helps in maintaining the stability of the track system by spreading loads from the sleepers uniformly across the bridge. It also provides a proper drainage system for water away from the rails and sleepers. The coarse stone particles have good properties to withstand and absorb shock from dynamic loads. At least 0.2 m depth of ballast is preferred to avoid damage to the bridge by repair machines and ensure uniform wheel load distributions.

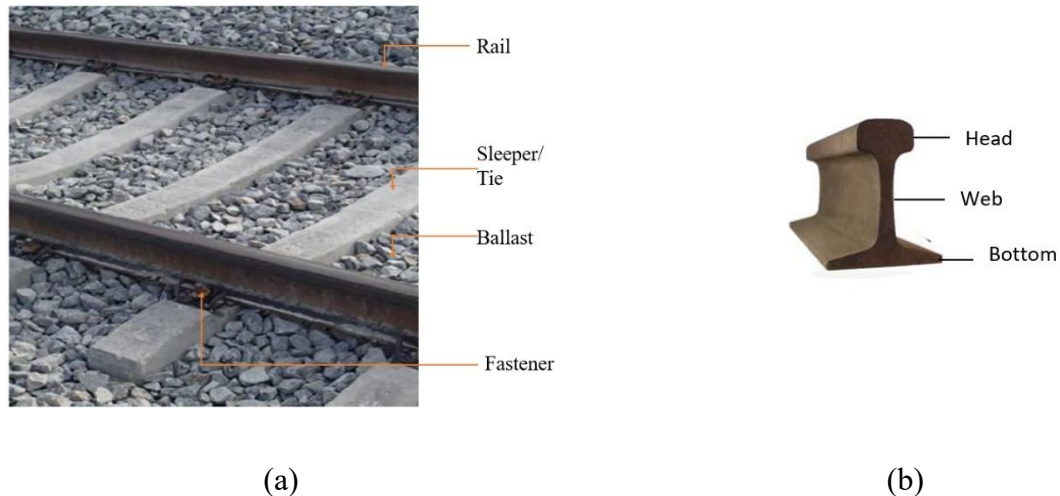


Figure 1.4 (a) Common components of railroad structure (b) Rail details

### 1.4. Railroad Bridges in the U.S.

The U.S. Rail network is one of the largest, safest, and most efficient transportation modes. Railroad bridges are the most critical components in the whole network. According to the analysis of the recent U.S. Department of Transportation’s (DOT) Bridge Inventory record, more than one-third, or 220,000 number of bridges out of total of 618,000, need structural repair, rehabilitation work, or replacement. Bridge inspections are done every 2 years. Bridge ratings are renewed when inspections are completed. There is an absolute need of calculating more precise structural capacity for railroad bridges (ARTBA, 2021).

The overall growth in the economy, as well as the population in the U.S., led to a significant expansion of railroad traffic levels by 1990s. The freight railroad system facilitates large volumes of freight movement cost-effectively (Kara, 2011). The U.S. freight rail network consists of 140,000 rail miles handled by seven Class I railroads with running income of more than \$433.2 million that covers 21 regional railroads, and 510 local railroads. The funding

partnerships have been increased to maintain and reconstruct railroad bridges in the whole USA. Due to increased investments and initiatives in the US rail system, there is always a demand for more research on the advancement and response of critical railroad structures (TxDOT, 2019).

There are approximately 100,000 railroad bridges in the U.S., among them 60% were built before 1950. The trend of increasing limits is very common for the railroad industry. Their key structural members are aging with the increased traffic density and the loads. There are always chances of unpredicted and catastrophic structural failures. One of the first high-speed train projects connecting Houston and Dallas cities in the United States has been proposed by Texas Central Partners, LLC with expected service beginning in early 2026. This rail line will have approximately 240 miles to travel in less than 90 minutes. So, considering such increased speed and evolving high-speed rail service, it is important to monitor the status of existing bridges and communicate potential failures well in advance.

### **1.5. Damage detection in railroad bridges**

Most of the railroad bridges are monitored by visual inspections which are sometimes unreliable and inconsistent due to human error. Identifying damage by measuring the change in dynamic response of railroad bridge in both time and frequency domains has become the increased area of interest. For this purpose, sensors can be installed on the bridge to measure acceleration responses and signals. These signals can be characterized by the Hilbert Huang Transform (HHT) which is a powerful method for identifying non-stationary and non-linear anomalies hidden in the time series signals. For example, acceleration of an OD railroad bridge is contaminated with the nonlinear effects caused by the axle's impact load.



Figure 1.5 Union Pacific train derailment due to broken rail on a Tempe, Ariz., bridge in July 2020 (source: FRA Factual Railroad Accident Report HQ-2020-1390 and Article by Johnny Diaz on The New York Times dated July 29, 2020)

Ultimately, this study intends to detect damage in an open deck steel truss railroad bridge under the moving train load using machine learning.

### **1.6. Objectives and Scope of the Work**

The overall objective of this research is to detect damage in an open deck steel truss railroad bridge with the impact of broken rail under moving train using machine learning methods. The specific objectives comprise of three tasks.

- i) Develop simple model of bridge with single and double axle moving load and validate the result with analytical solution. Then, develop an accurate model of existing steel truss railroad bridge and validate with field study.
- ii) Perform dynamic analysis with moving train load in different speeds for healthy and damaged bridge cases and get the response in terms of acceleration signal from different sensor locations.

ii) Employ machine learning classifier to detect and classify damage after the extraction of damage features from Hilbert Huang Transform. Ultimately, expand it to predict the condition of bridge effectively.

The system is linear in the state of geometry, material properties and boundary conditions. Cross sectional area is constant throughout the length. The number of concentrated loads represent the train axle loads. The damage has been considered at the mid-section of the bridge in the joint between stringer and cross girder. The broken rail is considered at the mid-point of the bridge for greater impact.

## CHAPTER II

### LITERATURE REVIEW

#### **2.1. Damage to Railroad Bridges**

The damage to railroad bridges due to moving load has been widely studied. Azim and Gul presented a method for element level damage detection of railroad truss bridges with the analysis of acceleration and strain data. The acceleration and strain time-history data were received from the field through the cluster of sensors during the passage of trains. A combined damage index was obtained from both acceleration and strain analysis and validated with a finite element (FE) model of a railroad truss bridge (Azim & Gül, 2021).

Zhao and Zhang produced structural damage identification method based on the change of modal data before and after the presence of damage. In this method, the assumption was that the reduction in structural stiffness due to damage is the summation of each element stiffness matrix times damage coefficient. The damage coefficient can then be solved alternatively from the equation of motion. Another term, the modal assurance criteria (MAC) was used to verify the correlation of mode shapes with the undamaged and the damaged structure. Numerical model of six-span truss beam was used to verify the method (Zhao & Zhang, 2012).

Mousavi et. al. studied the application of full ensemble empirical mode decomposition with adaptive noise technique to identify the damage on a steel truss bridge model built at laboratory with white noise excitations. The authors extracted key features from the intrinsic mode functions such as energy, instantaneous amplitude, unwrapped phase, and instantaneous frequency to localize and quantify the damage. Damage indices were also proposed based on two statistical time-history features namely kurtosis and entropy. The experimental results reveal the method to be better in addressing the damage detection compared to other available techniques (Mousavi et al., 2022).

Malekjafarian et. al. prepared training data set from an artificial neural network (ANN) using the vehicle responses measured from multiple passage over a healthy bridge. The Discrete Fourier Transform (DFT) plot of the acceleration was used to predict the response from its speed. The differences between the predicted and measured responses for each passage was calculated as a prediction error using root mean square error. To identify the changes in the feature, a damage indicator was outlined using a Gaussian process (Malekjafarian et al., 2019).

Rageh et. al. trained the ANN using bridge computational models to simulate damage scenarios. The procedure for generating training data was based on measured structural response from the numerical model. The efficiency and accuracy of damage detection methods were found to be significantly influenced by the level of modeling uncertainties (MUs). The authors investigated the applicability of the proposed framework to in-service bridges analyzing the effect of MUs. As per the results obtained, the damage location and intensity were detected accurately for the studied cases; however, accuracy reduced with the increase of MUs (Rageh et al., 2020).

Mehrjoo et. al. estimated the damage intensities of joints for truss bridges using back-propagation based neural network. The substructural identification method was utilized to solve the issues related to many unknown parameters. The neural network used natural frequencies and mode shapes as input parameters for damage identification. Numerical models were used for validating the accuracy and efficiency of the proposed method (Mehrjoo et al., 2008).

Onur Avci et al reviewed the studies on vibration based structural damage detection from traditional methods to Machine Learning and Deep Learning methods. They presented the main features of the traditional methods and a thorough review of the most recent ML and DL algorithms utilized for vibration-based structural damage detection (Avci et al., 2021).

Svendsen et al suggested an approach for identifying damaged joint in existing steel bridges. With the help of appropriate instrumentation, the methodology combined the use of temporal moments from the response measurements. Damaged joint connections are identified by comparing statistical parameters based on temporal moments to a baseline parameter evaluated for all considered joints. The method was found applicable to open-deck steel bridges and localization of damaged joint is performed by applying the instrumentation framework (B. Svendsen et al.,2020).

The beam element model is the simplest form of bridge model. The dynamic responses of bridges under train loads can be modeled the train as a point load and the bridge as a simple Euler-Bernoulli beam. For a beam traversed by a single load, the mass of the beam is negligible compared to the moving load. Many researchers proposed analytical solutions for simplified and fundamental problems, with some variations on the moving force. At the instance of load arrival, the beam is at rest, thus possesses neither deflection nor velocity. There are some research which have studied moving loads to simulate trains with multiple cars for single and multi-span beams.

Moving load model does not consider the inertia effect of the moving vehicle, so these are valid only when the mass of the vehicle is small relative to the mass of the bridge.

Zhongquan et al., 2009, studied the static behavior of a reinforced concrete small span railway bridge using finite element method. The load distribution was studied in the support and in bearings, and similarly the effect of the stress distribution was also studied. The analysis results were validated with the field load testing results. The result showed that the influence of load distribution was not significant, while those of supporting width and additional support were considerable; and the spatial effect was also found to be significant (Zhongquan et al., 2009).

The numerical analysis for railway bridges is time consuming because of the complexity of load configurations and increased speed of high-speed trains. For practical purposes and time efficient simulation, simplified models of bridge, track and train are always preferred. One of the railway bridges in Stockholm named “New Arsta Railway Bridge” was taken for this study. The simplified Bernoulli-Euler beam element FE model was initially adjusted based on static load. Most influencing parameters in modeling were identified and optimized in FE model using statistical identification. To validate the model, several static and dynamic field tests were done with a loaded train. The systems were found to work efficiently. It was found that the complex bridge can be simplified by beam theory and corresponding equivalent modulus of elasticity for reliable results. The equivalent modulus of elasticity for the concrete grade was found to be 25% larger than the specified mean value. The moving load was simulated with high-speed train loads in the optimized FE model. The vertical acceleration of the bridge deck was much below the allowable value. So, multi-span continuous concrete bridges are not so sensitive to train induced vibrations but may be suitable for high-speed trains. The appropriate area of introducing simple FE model with updated procedure was addressed by the study. (Wiberg, n.d.)

Baniya Surendra, 2015 used Devon truss railroad bridge over Housatonic River in Milford to determine dynamic response under moving trains. Natural frequencies and displacements were compared with the field test data. The authors studied the effects of different modes in vertical response of bridge and did analysis for 40 MPH speed for three different trains. Among the three trains studied, they found Amtrak Accela train giving the highest response in terms of vertical and lateral displacement in every mode.

Differential settlement has been found as one of the major issues in the rail industry at stiffness transition points between bridge and road interface. In this study, the authors used a coupled multibody and finite element method to find rail settlement. Wheel-rail contact is found based on Hertzian penalty formulation. The model was decomposed into different linear model of track substructure such as rails, fasteners, sleepers, ballast, sub-ballast, and subgrade to improve the efficiency. To feed into a nonlinear FEA model, the contact forces between the wheel and rail are obtained from the multibody simulation that determines the settlement of the soil. In this way, an elasto-viscoplastic soil model is presented to determine the permanent settlement of the soil. As the yield is small, the linear stiffness of the multibody model is still relatively accurate. The simulations can be used to help find settlement and assess mitigation techniques. (Foster & Kulkarni, 2021)

Although extremely complex vehicle, track, and bridge models can be derived to represent the real condition, simpler models are still well used to identify the key parameters controlling the railroad bridge responses. The speed parameter, which is a non-dimensional property that is adopted to demonstrate the relationship between the speed of the vehicle and the responses of the bridge, is computed.

Ticona Melo et al. studied one of the railway bridges to standardize the numerical model considering the interaction among the vehicle, rail and the bridge deck. Sensors were placed at different critical points of the structure to measure ambient vibration and computed the modal parameters. The behavior of the system was identified and tested after comparing the experimental with numerical values. During modeling, the deficiency in the ballast material was found in between the half-decks at the boundaries of longitudinal joint. A correction factor was determined to adjust experimental and numerical values on the displacements and accelerations. Regarding deck accelerations, the damping coefficients were found to be critical. (Ticona Melo, Ribeiro, et al., 2020)

There are very few studies which focus primarily on the dynamic response of the railway bridge. This study provided some modelling choices for the train-bridge interface. The important factors are recognized for study and provided basis to determine an appropriate degree of complexity in modelling interaction between train and bridge. The responses in terms of interaction between train and bridge are compared changing other key parameters. The authors observe the combination of these parameters to reduce the bridge response. (Arvidsson & Karoumi, 2014)

Ping Lou used the finite element method for dynamic analysis of bridge-track-train interaction. The author modeled the set of wheels by a mass-spring-damper system. The rails and decks were modeled as Bernoulli-Euler beam elements. Similarly, the elasticity and damping of the rail were modeled as continuous springs and dampers. The validation of the suggested method is shown by a comparison of numerical value with the existing literature. Two vehicle models were used to identify the effects on different bridge models. The damping values

of bridges were also varied for the maximum dynamic responses of train, track, and bridges.  
(Lou, 2007)

The dynamic behavior of the critical zone at transition between a bridge and open track was studied for a moving train using a two-dimensional finite element approach. The effect of different layers and backfills on the track behavior was studied. It was evaluated that the reduced sleeper spacing improved the performance of the critical zone. The numerical model was confirmed with the field data mentioned in the previous literature. The subgrade soil significantly affects the track response on the outer side of the critical zone. One side after entering the bridge is stiffer and another side above subgrade soil is softer. Once the subgrade becomes stiffer and stronger, the contribution of the ballast and sub ballast to the overall track displacement increases. It was found that the track stiffness was significantly increased with wedge shaped backfill (Punetha et al., 2021)

Yang et al., 2004 did analytical study of the resonance and cancellation phenomena of elastic support bridges caused by a sequence of moving loads at constant interval. The resonance condition in terms of different speeds is the same for the beam with both the elastic and simple supports. As the elastic support beam has a lower frequency of vibration, it has a lower resonant speed; due to which it can be more easily excited than simply supported beams. The speed parameter for the cancellation condition to occur increases slightly as the stiffness ratio increases. However, since the frequency of vibration is slightly smaller for an elastically supported beam, it turns out that the real cancellation speed for an elastically supported beam remains close to that for the simply supported beam. Whenever the cancellation speed comes close to or coincides with the resonance speed, the phenomenon of resonance will be suppressed. The cancellation condition is more decisive than the resonance condition. Once a resonance

condition is reached for an elastically supported beam, much larger peak responses will be induced on the beam, compared with those of the simply supported beam.

## **2.2. Effects of Wheel-Rail Contact**

Rail is a critical component that directly carries the impact of train load. Under the long-term service and the effect of train load, the rails are subject to various damages. The broken rail has a significant impact on wheel-rail contact and running safety of trains. Once the rails are broken, the continuity of rails are damaged. The discontinuity caused by the broken rail results in the loss of torsional stiffness. During the passage of wheel over the broken rail, a strong dynamic force of wheel-rail impact will be excited, exacerbating the wheel-rail contact and vibration of rail. In addition, the broken rail can cause derailment and ultimately catastrophic structural failure in the railroad bridge structure (Gao et al., 2021).

Ticona Melo, Malveiro, et al., 2020 studied the non-linear actions of the track-deck connections having irregularities in the track. A specific finite element model was developed with a track-deck interface, having a group of a friction contact element and a non-linear spring. The longitudinal resistance of the track is changed, based on the locations of loads. The findings indicated that especially for medium and large span bridges, the effects of temperature variations influenced the responses of the track-deck interface rather than the live loads. Under train live loads, the extension of the regions with plastic actions were extended with the change in the horizontal stiffness of the support. The plastic hinge was found to be extended upto 55% of span for medium and large span bridges. The evaluation of the plastic attacks was achieved at the track-deck interface for different types of bridges. Reduced stiffness ultimately causes the increase in vertical movements of the bridge (Ticona Melo, Malveiro, et al., 2020).

The simulation of local irregularity showed that at the time of deterioration of harmonic local irregularity, even if the amplitude is small, there is serious deterioration of wheel-rail with strong shock and vibration. The amplitude of harmonic local irregularity is directly proportional to the maximum wheel-rail vertical force. When deterioration of the amplitude exceeds a certain value or limit derailment happens. The wheel-rail dynamic interaction also increases with increasing speed. Considering constant speed, harmonic local irregularity settlement deterioration and harmonic local irregularity raised deterioration increases the maximum wheel-rail vertical force by 14.4%. So, local irregularity deterioration and the speed of the locomotive are found to be controlling factors. (Chen et al., 2014)

If a derailment occurs on railroad bridges, especially at high speeds, it may cause significant damage to the life and properties. There is always the probability of a train being exposed to natural hazards while it is running over a structure such as bridge. This paper presents a comprehensive literature review of the issues with the train running safety assessment on railroad bridges for the assessment of the derailment risk (Montenegro et al., 2021).

### **2.3. Structural Health Monitoring of Railroad Bridges**

The main objectives of Structural Health Monitoring are to identify damage in the structure at its real-time and prompt action can be made to keep the structures operational and safe. For these reasons, there is an increased demand for smart approaches which can support decision-making for maintenance of structures. These are based on a cost-effective and reliable monitoring system which is called Structural Health Monitoring.

The author intends to provide an approach to Structural Health Monitoring of bridges which focuses on damage detection using data-based methods. The data is collected in healthy as well as damaged states of the structure. Then the data collected under the healthy state is used for training Artificial Neural Networks, as the primary algorithm of the proposed method. Afterwards, new data collected under healthy or damaged states can be directly compared with the corresponding projections. Finally, Artificial Neural Networks for the assessment of structural condition is appropriately used. This is put into effect by adjustments to enhance the performance of the algorithm. This research work intends to contribute for proactive maintenance by which data is continuously collected and analyzed in almost real-time to support decision-making (Neves, n.d.).

Physics based approach to Structural Health Monitoring (SHM) has practical shortcomings such as conditions of simple structure under controlled environments. Sensors and sensor networks were being utilized to collect data. Lack of sensor data corresponding to different damage scenarios continues to remain a challenge. Most of the supervised Machine Learning, when trained using limited data, lack robustness and generalizability. In this study, physics informed learning (integration of domain knowledge) in to learning process is presented (Neves, n.d.).

## **2.4. Machine Learning Classification**

The railroad industry needs to explore the potential of applying artificial intelligence and machine learning in bridge structures because machine learning is capable of handling complex problems with high computational efficiency. This can assist stakeholders in decision making process. The damage detection in an open deck steel truss railroad bridge with proper extraction

of features using machine learning is yet to be properly addressed. This study offers the extent to machine learning applications in damage detection of railroad bridges. The critical task in generating any Machine Learning algorithm is to gather enough reliable data to prove suitable metrics, with most of this data being used for training and validation purposes. After training the machine learning model correctly, it expands itself to be able to forecast effectively and can make decisions.

Chalouhi et al., 2017 detected and localized damage in railway bridges using machine learning. For this study, air temperature and deck acceleration data were measured. The major stages of the study are collection of data in reference condition, preprocessing of acceleration time histories and aimed at extracting crossing train characteristics (speed, running direction and number of axles), Training of ANN using data collected in reference condition and health classification of bridge in current condition comparing predicted and measured responses. A set of neural networks are trained to predict deck acceleration under every environment and operational condition. The responses are compared with acceleration predicted. Changes in behavior due to damage are detected as discrepancy between predicted and measured responses. The study has shown good agreement with the results from previous studies based on mode shape variation. Ultimately it confirmed the possibility of applying machine learning to real bridges (Chalouhi et al., 2017).

There are different types of sensors used in structural health monitoring of Railroad Bridges. Different applications are used for sensors such as electrical, optical, geodetical and acoustical. A lot of parameters like displacement, stress and strain can be supervised using sensors. Some conventional sensors to measure displacement and accelerations are strain gauges and accelerometers. However, fiber optic sensors and lasers are available as modern and efficient

sensors. They are easy to install and can collect data with very less human effort automatically, which saves a lot of time. For railway bridges these days, remote monitoring can be the only way to monitor a structure. (Enckell, 2006)

To improve the accuracy and efficiency of damage detection methods, bridge response data collected from the embedded sensors in the model has been intended to be used for machine learning. These computational resources open the opportunity for monitoring and control applications to use computing approaches beyond traditional methods to data-driven by means of machine learning (Hou et al., 2022).

In this work, a data-driven damage detection approach that considers the true behavior of a bridge is proposed. The approach is based on the bridge dynamic response data due to a standard train loading, identify features and make decisions with minimal human interventions.

In this study, typically the finite element model (FEM) of the railroad bridge in SAP 2000, has been utilized and validated with field data. Despite relying on the physical model of the structure, the model is dependent on statistical pattern recognition (PR), which is used by machine learning algorithms (Malekloo et al., 2021).

## **2.5. Limitations of the Previous Research**

Several studies have been performed to improve the identification and detection of damage in different types of bridges. However, none of these studies, to the best of the author's knowledge, have presented damage detection in an open deck steel truss railroad bridges using proper feature extraction technique such as HHT and classification of damage using machine learning. There is sufficient potential of applying machine learning in monitoring and detecting

damage in railroad bridge structures because it has the capability of handling complex problems with high computational efficiency. This study focuses on the damage detection of typical open deck steel truss railroad bridge using Hilbert Huang Transform for feature extraction and Machine Learning for classification. Impact of broken rail on bridge damage detection has also been considered. Ultimately, machine learning will be used to identify and classify the status of the bridge.

## CHAPTER III

### THEORY OF VIBRATION OF A SIMPLY SUPPORTED BEAM SUBJECTED TO MOVING LOADS

#### 3.1. Mathematical Formulation of moving load

##### 3.1.1. Effect of Single Axle Load

In this section, a simply supported beam bridge with finite element model has been presented and validated with analytical solution. A single span simply supported railroad bridge subjected to single axle load ( $P$ ) moving at constant speed ( $V$ ) can be simplified with the assumption of linear elastic model. The bridge is assumed to have uniform cross section with constant mass and  $EI$  values.

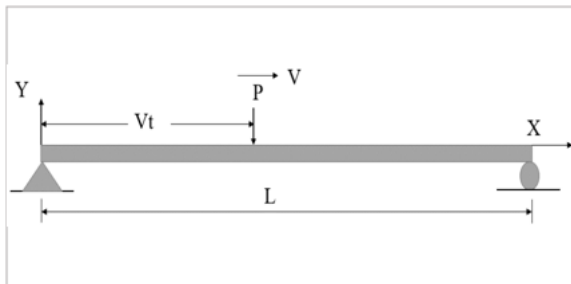


Figure 3. 1 Simply supported bridge subjected to a constant single axle moving load

The analytical solutions for the vertical displacement of the above simply supported single span bridge can be derived as follows.  $u(x, t)$  is the displacement of the beam along the  $y$

axis at position  $x$  and time  $t$ ,  $L$  the length of the bridge,  $m$  the mass per unit length,  $c_e$  the external damping coefficient,  $c_i$  the internal damping coefficient,  $E$  the modulus of elasticity, and  $I$  the moment of inertia of the bridge. During simplification process, following assumptions are made for the computation equally considering the accuracy.

i) The bridge is homogeneous and having constant cross section, ii) only one moving load at a time is allowed on the bridge, iii) only the force is considered, and the inertia effect is neglected, iv) speed  $v$  is constant throughout the bridge, v) the bridge is initially at rest vi) surface irregularity of the bridge and track is not considered.

The equation of motion of a simply supported beam traversed by a force  $p$  at constant speed  $v$  is given by.

$$mu + c_e u + c_i I u'''' + E I u'''' = P \delta(x - vt), \quad 0 \leq vt \leq L \quad (3.1)$$

Where, primes (') and dots (·) denote differentiation with respect to coordinate  $x$  and time  $t$ , respectively, and  $\delta$  is the Dirac delta function. The boundary conditions are.

$$u(0, t) = 0, \quad u(L, t) = 0, \quad E I u''(0, t) = 0, \quad E I u''(L, t) = 0$$

The beam is assumed to be at rest prior to the arrival of the moving vehicle so the initial conditions are.

$$u(x, 0) = 0, \quad \dot{u}(x, 0) = 0$$

The transverse deflection of the beam  $u(x, t)$  due to only the  $n$ th mode of vibration can be written as,

$$u(x, t) = \phi_n(x) q_n(t) \quad (3.2)$$

Where,  $\Phi_n$  is the nth vibration mode which satisfies boundary conditions.  $q_n(t)$  represents the generalized coordinate for nth vibration mode.

Substituting value of equation (3.2) in equation (3.1), Multiplying both sides of Eq. (3.1) by  $\Phi_n$  and integrating with respect to  $x$  from 0 to  $L$ , the generalized equation of motion of the beam is obtained as

$$\begin{aligned}
 m q_n(t) \int_0^L [\Phi_n(x)]^2 dx \\
 + q_n(t) \times \left\{ c_e \int_0^L [\Phi_n(x)]^2 dx + c_i I \int_0^L \Phi_n^{(4)}(x) \Phi_n(x) dx \right\} \\
 + EI q_n(t) \int_0^L \Phi_n^{(4)}(x) \Phi_n(x) dx = p \Phi_n(vt)
 \end{aligned} \quad (3.3)$$

Where,

$$\int_0^L \delta(x - a) \Phi_n(x) dx = \Phi_n(a)$$

$$\int_0^L \delta(x - a) \Phi_n(x) dx = \Phi_n(a)$$

Let us denote the vibration frequency  $\omega_n$  of the nth mode of the beam as

$$\omega_n^2 = \frac{EI \int_0^L \Phi_n^{(4)}(x) \Phi_n(x) dx}{m \int_0^L [\Phi_n(x)]^2 dx} \quad (3.4)$$

We can write,  $c_e = \alpha_e m$ , and  $c_i = \alpha_i E$  and  $\xi_n$  is the corresponding damping coefficient for  $n^{\text{th}}$  mode of vibration given by,

$$\xi_n = \frac{1}{2} \left( \frac{\alpha_e}{\omega_n} + \alpha_i \omega_n \right)$$

Then equation (3.3) becomes

$$q_n + 2\xi_n \omega_n q_n + \omega_n^2 q_n = \frac{p \phi_n(vt)}{\int_0^L m [\phi_n(x)]^2 dx} \quad (3.5)$$

This equation of motion is valid only when the acting position  $vt$  of the moving load is located within the beam, i.e.,  $0 \leq vt \leq L$ . Once the moving load leaves the beam, only free vibration remains.

For a simply supported beam, the  $n^{\text{th}}$  mode shape of vibration is

$\phi_n(x) = \sin \frac{n\pi x}{L}$  and the frequency of vibration  $\omega_n$  obtained from Eq. (3.4) is

$$\omega_n = \frac{n\pi}{L} \sqrt{\frac{EI}{m}}$$

Substituting the value into Eq. (3.5) yields the equation of motion for the  $n^{\text{th}}$  mode of the simply supported beam as

$$q_n + 2\xi_n \omega_n q_n + \omega_n^2 q_n = \frac{2p}{mL} \sin \frac{n\pi vt}{L} \quad (3.6)$$

which is uncoupled from the other modes of vibration. From this equation, the generalized coordinate of  $q_n$  for the  $n^{\text{th}}$  mode can be solved as

$$\begin{aligned}
q_n = & \frac{2pL^3/(EI_n^4\pi^4)}{(1 - S_n^2)^2 + (2\xi_n S_n)^2} \\
& \times \left\{ (1 - S_n^2) \sin \Omega_n t - 2\xi_n S_n \cos \Omega_n t \right. \\
& + e^{-\xi_n \omega_{dn} t} \left. \left[ 2\xi_n S_n \cos \omega_{dn} t + \frac{S_n}{1 - \xi_n^2} (2\xi_n^2 + S_n^2 \right. \right. \\
& \left. \left. - 1) \sin \omega_{dn} t \right] \right\} \tag{3.7}
\end{aligned}$$

Where,  $\omega_{dn}$  is the damped frequency of vibration of the beam and given by

$$\omega_{dn} = \omega_n \sqrt{1 - \xi_n^2}$$

$\Omega_n$  is the excitation frequency.

$$\Omega_n = \frac{n\pi v}{L}$$

$S_n$  is the non-dimensional speed parameter defined as the ratio of the frequency of excitation of the moving load to the  $n$ th frequency of vibration of the beam

$$S_n = \frac{\Omega_n}{\omega_n} = \frac{n\pi v}{\omega_n L} \tag{3.8}$$

Consequently, the total displacement  $u(x, t)$  of the beam caused by all the vibration modes can be summed as follows:

$$\begin{aligned}
u(x, t) = & \sum_{n=1}^{\infty} \frac{\frac{2pL^3}{EI\pi^4}}{(1 - S_n^2)^2 + (2\xi_n S_n)^2} \\
& \times \left\{ (1 - S_n^2) \sin \Omega_n t - 2\xi_n S_n \cos \Omega_n t \right. \\
& + e^{-\xi_n \omega_n t} \left[ 2\xi_n S_n \cos \omega_{dn} t \right. \\
& \left. \left. + \frac{S_n}{1 - \xi_n^2} (2\xi_n^2 + S_n^2 - 1) \sin \omega_{dn} t \right] \right\} \times \sin \frac{n\pi x}{L}
\end{aligned} \tag{3.9}$$

This is the solution for displacement of the beam caused by a single moving load with considering the effect of damping.

In the above Eq. (3.9), the terms containing  $\Omega_n t$  represents the forced vibration of the bridge induced by the moving load, and the terms with  $\omega_{dn} t$  are the free vibration. This equation applies within the limit of the beam length. After the load has passed, the response is a free vibration with initial conditions equal to the conditions in the beam at the moment when the force leaves the span.

Practically, the effect of damping on the bridge is so small, due to the short acting time of the moving loads. So, it can be ignored completely. By neglecting the effect of damping, the total displacement  $u(x, t)$  can be written as;

$$u(x, t) = \frac{2pL^3}{EI\pi^4} \sum_{n=1}^{\infty} \frac{1}{n^4} \sin \frac{n\pi x}{L} \times \left( \frac{\sin \Omega_n t - S_n \sin \omega_n t}{1 - S_n^2} \right) \tag{3.10}$$

This is the equation of displacement of the simple beam at section  $x$  subjected to the moving load  $p$  acting at position  $vt$  without damping effect.

The result obtained for the midpoint displacement by considering the first mode only is sufficient, because all the anti-symmetric modes of vibration have zero contribution to the midpoint displacement. This gives the sense of using only the first mode which can yield generally good approximate solutions for vehicle-induced response (Yang et al., 2004).

### 3.1.2. Impact Factor for Midpoint Displacement

The results presented in this section cover a wide range of applications, as they are all expressed in terms of the nondimensional speed parameter.

The impact response induced by a single moving load on the beam is generally larger than that induced by multi or continuous moving loads due to the suppression effect of the simultaneous acting loads. Thus, the impact formulas for a single moving load should be regarded as reasonable higher value for the responses considered.

Impact factor,  $I$  can be given by.

$$I = \frac{u_d(x) - u_s(x)}{u_s(x)} \quad (3.11)$$

Where,  $u_d(x)$  and  $u_s(x)$  are the maximum dynamic and static response of the bridge at section  $x$  due to moving load.

For a simple beam, both the maximum dynamic and static displacement occur at the midpoint. The maximum static displacement of the beam under the static load  $p$  is given as,

$$u_s(L/2) = pL^3/48EI$$

Whereas the dynamic response for the midpoint displacement of the beam can be obtained from Eq. (3.10) by plugging the value of  $x = L/2$ ,

$$u_{\frac{L}{2},t} = \frac{2pL^3}{EI\pi^4} \sum_{n=1}^{\infty} \frac{1}{n^4} \sin \frac{n\pi}{2} \times \left( \frac{\sin \Omega_n t - S_n \sin \omega_n t}{1 - S_n^2} \right) \quad (3.12)$$

With these substitution, for  $n = 2, 4, \dots$  the shape function  $\sin(n\pi/2)$  become extinct at the midpoint, as it turns out to be asymmetrical. Thus, only the modes with  $n = 1, 3, \dots$  i.e., the symmetrical modes, contribute to deflection of the midpoint.

Likewise, the impact factor for the midpoint deflection of the simple beam caused by the moving load  $p$  acting at position  $vt$  is

$$I_u = \frac{96}{\pi^4} \sum_{n=1}^{\infty} \frac{1}{n^4} \sin \frac{n\pi}{2} \times \left( \frac{\sin \Omega_n t - S_n \sin \omega_n t}{1 - S_n^2} \right) \quad (3.13)$$

This term is independent of the magnitude  $p$  of the moving load. As there are contribution of higher order terms decreased by a factor  $n^{-4}$ , the effect of higher order terms in equation (3.13) can be neglected. We can also say that  $96/\pi^4 = 1$ .

Then the equation (3.13) becomes

$$I_u \cong \left( \frac{\sin \Omega_1 t - S_1 \sin \omega_1 t}{1 - S_1^2} \right) \quad (3.14)$$

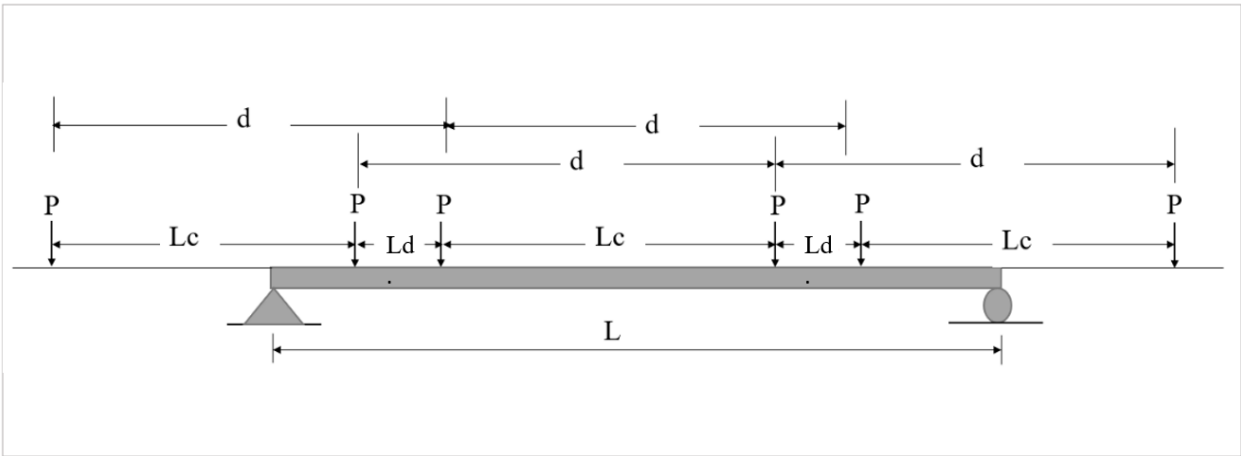
The impact factors for the midpoint displacement can be calculated using Eqs. (3.13) and (3.14), considering either multi-modes or the first mode only. The midpoint displacement impact response of the simple beam is dominated by the first mode (Yang et al., 2004).

### 3.1.3. Effects of Series of Moving Loads

A train is modeled representing two sets of moving loads at constant intervals. To simplify the solution within the range of accuracy, bridge and track irregularities are not considered.



(a)



(b)

Figure 3. 2 Simply supported railroad bridge subject to (a) series of moving loads (b) actual train loads

The train is supposed to have  $N$  number of identical cars, and each car is supported by two bogies and two axles. Let us consider  $L_c$  as the distance between the two axles of a car, and

$L_d$  as the distance of axles between two cars. A train has been represented as a series of moving wheel loads  $p$ . We can see a time lag of  $L_c/v$  between the two sets of moving loads. Based on the above configuration, the wheel load function  $F(t)$  for the train can be given as.

$$F(t) = \sum_{j=1}^N P \times U_j(t, v, L) \quad (3.15)$$

Where,

$$U_j(t, v, L) = \delta[x - v(t - t_j)] \times [H(t - t_j) - H(t - t_j - \frac{L}{v})] \quad (3.16)$$

$\delta$  is dirac delta function,  $x$  is coordinate of the beam,  $H$  is step function,  $t_j$  is arriving time of the  $j^{\text{th}}$  load at the beam,  $t_j = (j - 1)d/v$ , and  $N$  - total number of moving loads.

The action of the  $j^{\text{th}}$  moving load is effective by the term  $H(t-t_j)$  once entering the beam, and will be disabled by the term  $H(t - t_j - L/v)$  while it leaves the beam.

Then equation (4.15) can be modified to.

$$F(t) = \sum_{j=1}^N P \times [U_j(t, v, L) + U_j(t - t_c, v, L)] \quad (3.17)$$

This is applicable once neglecting the effect of inertia of the moving masses and the train bridge interaction. Again, the forcing function  $F_n(t)$  for the  $n^{\text{th}}$  generalized coordinate can be given by

$$F_n(t) = \frac{2P}{mL} \sum_{j=1}^N [f_n(t, v, L) + f_n(t - t_c, v, L)] \quad (3.18)$$

If only the effects of moving loads are considered, the equation of motion in terms of generalized coordinate  $q_n$

$$q_n + 2\xi_n \omega_n q_n + \omega_n^2 q_n = F_n(t) \quad (3.19)$$

$$q_n(t) = \frac{1}{m\omega_{dn}} \int_0^t F_n(\tau) e^{-\xi_n \omega_n (t-\tau)} \times \sin \omega_{dn}(t-\tau) d\tau \quad (3.20)$$

$$= \frac{2PL^3}{EI\pi^4} [P_n(v, t) + P_n(v, t - t_c)]$$

where  $\omega_{dn}$  is the damped frequency of vibration of the beam given by

$$\omega_{dn} = \omega_n \sqrt{1 - \xi_n^2}$$

The function  $P_n(v, t)$  can be expressed as

$$P_n(v, t) = \frac{1}{n^4} \sum_{j=1}^N \frac{1}{(1 - S_n^2)^2 + 4(\xi_n S_n)^2} \quad (3.21)$$

$$\times A \times H(t - t_j) + (-1)^{n+1} \times B \times H\left(t - t_j - \frac{L}{v}\right)$$

Here the value of A and B are found as,

$$A = (1 - S_n^2) \sin \Omega_n(t - t_j) - 2\xi_n S_n \cos \Omega_n(t - t_j)$$

$$+ e^{-\xi_n \omega_n (t-t_j)}$$

$$\times \left[ 2\xi_n S_n \cos \omega_{dn}(t - t_j) + \frac{S_n}{1 - \xi_n^2} (2\xi_n^2 + S_n^2 - 1) \sin \omega_{dn}(t - t_j) \right] \quad (3.22)$$

$$\begin{aligned}
B = & \left(1 - S_n^2\right) \sin \Omega_n \left(t - t_j - \frac{L}{v}\right) - 2\xi_n S_n \cos \Omega_n \left(t - t_j - \frac{L}{v}\right) \\
& + e^{-\xi_n \omega_n \left(t - t_j - \frac{L}{v}\right)} \\
& \times \left[ 2\xi_n S_n \cos \omega_{dn} \left(t - t_j - \frac{L}{v}\right) + \frac{S_n}{1 - \xi_n^2} (2\xi_n^2 + S_n^2 \right. \\
& \left. - 1) \sin \omega_{dn} \left(t - t_j - \frac{L}{v}\right) \right]
\end{aligned} \tag{3.23}$$

Where,  $\Omega_n$  denotes the exciting frequencies of the moving loads,  $\Omega_n = n\pi v/L$ , and the speed parameter,  $S_n = n\pi v/(\omega_n L)$ .

The terms  $P_n(v, t)$  and  $P_n(v, t - t_c)$  in Eq. (3.20) represent the dynamic responses excited by the two sets of wheel loads, and the second set has a time lag  $t_c$  after the front set of loads.

Neglecting the effect of damping and considering only the first mode of vibration, the dynamic response of the beam can be derived as

$$u(x, t) = \frac{2pL^3}{EI\pi^4} \times \frac{1}{1 - S_n^2} \sin \frac{\pi x}{L} [P_1(v, t) + P_1(v, t - t_c)] \tag{3.24}$$

where the response function  $P_1(v, t)$  for the first set of wheel loads is given by.

$$\begin{aligned}
P_1(v, t) = & \sum_{k=1}^N \left\{ [\sin \Omega_1(t - t_j) - S_1 \sin \omega_1(t - t_j)] \times H(t - t_j) \right. \\
& + \sin \Omega_1 \left(t - t_j - \frac{L}{v}\right) \\
& \left. - S_1 \sin \omega_1 \left(t - t_j - \frac{L}{v}\right) \times H\left(t - t_j - \frac{L}{v}\right) \right\}
\end{aligned} \tag{3.25}$$

The terms  $P_1(v, t)$  and  $P_1(v, t - t_c)$  denote the contribution of the front and rear wheel loads, respectively.

Depending on the bridge/car length ratio  $L/d$ , there may be different number of wheel loads or no loads acting on the railroad bridge during the passage of the train. So, The most severe case occurs when the front wheel load of the  $(N - 1)^{\text{th}}$  car has left the bridge, and the front wheel load of the  $N^{\text{th}}$  car has entered the bridge, namely, when the rear wheel load of the  $(N - 1)^{\text{th}}$  car and the front wheel load of the  $N^{\text{th}}$  car are simultaneously acting on the bridge.

The dynamic response of the beam has been excited to the maximum by the former  $N - 1$  cars that have passed the bridge. For this case,  $t_N < t < (t_N + L/v)$  and the equation (3.25) becomes

$$\begin{aligned}
 P_1(v, t) = & \left[ \sin \Omega_1(t - t_N) - S_1 \sin \omega_1(t - t_N) \right] \times H(t - t_N) \\
 & - 2S_1 \cos \frac{\omega_1 L}{2v} \times \sin \omega_1 \left( t - \frac{L}{2v} \right) \\
 & + \sin \omega_1 \left( t - \frac{L}{2v} - \frac{t_N}{2} \right) \times \frac{\sin \omega_1 \left( \frac{t_N}{2} - \frac{d}{2v} \right)}{\sin \frac{\omega_1 d}{2v}} \times H \left( t - t_{N-1} - \frac{L}{v} \right)
 \end{aligned} \tag{3.26}$$

The term containing  $H(t - t_N)$  represents the dynamic response of the beam induced by the motion of the  $N^{\text{th}}$  front wheel load of the train, and the term containing  $H(t - t_{N-1} - L/v)$  is the free vibration caused by the former  $N-1$  front wheel loads that have passed the bridge.

Since the two response functions  $P_1(v, t)$  and  $P_1(v, t - t_c)$  are similar in nature, only the function  $P_1(v, t)$  for the first set of wheel loads are considered in the above equation (3.26).

### 3.1.4. Resonance Conditions

The response of the simply supported beam will be maximum when the denominator of the second term of equation (3.26) is zero.

$$\text{Hence we can say, } \sin \frac{\omega_1 d}{2v} = 0; \quad \text{or} \quad \frac{\omega_1 d}{2v} = i\pi \quad \text{for } i = 1, 2, 3, \dots$$

This is the condition for resonance of the beam to occur under repetitive loads. For this condition, the response function  $P_1(v, t)$  in Eq. (3.26) turns out to be indeterminate.

By the relation  $t_N = (N - 1)d/v$  and L'Hospital's rule, it can be shown that

$$\sin \omega_1 \left( t - \frac{L}{2v} - \frac{t_N}{2} \right) \times \frac{\sin \omega_1 \left( \frac{t_N}{2} - \frac{d}{2v} \right)}{\sin \frac{\omega_1 d}{2v}} = (N - 2) \sin \omega_1 \left( t - \frac{L}{2v} \right) \quad (3.27)$$

Accordingly, the response will be as per following equation.

$$\begin{aligned} P_1(v, t) = & \left[ \sin \Omega_1(t - t_N) - S_1 \sin \omega_1(t - t_N) \right] \times H(t - t_N) - 2S_1(N \\ & - 1) \cos \frac{\omega_1 L}{2v} \times \sin \omega_1 \left( t - \frac{L}{2v} \right) \times H \left( t - t_{N-1} - \frac{L}{v} \right) \end{aligned} \quad (3.28)$$

This is the response case when the Nth wheel load is acting on the beam and the N-1<sup>th</sup> wheel load has already passed the beam. The last term containing  $H(t - t_{N-1} - L/v)$  indicates that under the condition of resonance, the response of the beam will be continuously advanced with more loads passing the beam.

For resonance condition, the critical car length  $d$  of the train traveling over the beam can be given as,

$$d = 2i \frac{\pi v}{\omega_1} = 2i S_1 L \quad \text{where, } i = 1, 2, 3, \dots$$

We have the car length  $d$  and beam span length  $L$ , the speed parameter  $S_1$  can be found from the resonance condition as

$$S_1 = \frac{d}{2iL} \quad \text{where, } i = 1, 2, 3 \dots \dots \dots$$

We can see from the relation that if the beam is longer, the speed for resonance will occur at lower value. Substituting the values of  $i = 1, 2, 3 \dots$  from the above equation, resonance may occur at the following speeds:  $S_1 = 0.50d/L, 0.25d/L, 0.167d/L, 0.125d/L, \dots$ , with declining values.

Here, the speed at  $0.5 d/L$  is the primary resonant speed, and all the remaining are the secondary resonant speeds (Yang et al., 2004).

### 3.1.5. Condition of Cancellation

In the Equation (3.26), if  $\cos(\omega_1 L/2v) = 0$ ; the excitation effects of all the former  $N - 1$  wheel loads passed over the beam will be equals to zero. In this case, no remaining response will be developed by the loads that passed through the beam. Such a condition is called the condition of cancellation. Then the response function  $P_1(v, t)$  will be.

$$P_1(v, t) = [\sin \Omega_1(t - t_N) - S_1 \sin \omega_1(t - t_N)] \times H(t - t_N) \quad (3.29)$$

This equation (3.29) indicates that if the condition of cancellation is happened, the response of the beam is determined by the last wheel load ( $N^{\text{th}}$  load) acting on the beam, as the free vibrations produced by all the former wheel loads have been cancelled.

Moreover, at the condition of cancellation, no remaining response will be seen on the beam after the last wheel load passes the beam.

We know that  $S_1 = \pi v / (\omega_1 L)$ , for the condition of cancellation, the speed parameter can be determined as:

$$S_1 = \frac{1}{2i - 1} \quad \text{where, } i = 1, 2, 3 \dots \dots \dots$$

From the above equation, the cancellation can be found at speed parameters,  $S_1 = 1, 1/3, 1/5, \dots$ . From the equation (3.26) we can see that the condition of cancellation is more significant and dominant than resonance.

### 3.2 Validation of the Moving Load Model in SAP2000

#### 3.2.1. Single Axle Load

This simple moving load example was taken for the validation of the model because it is also possible to check and validate analytically.

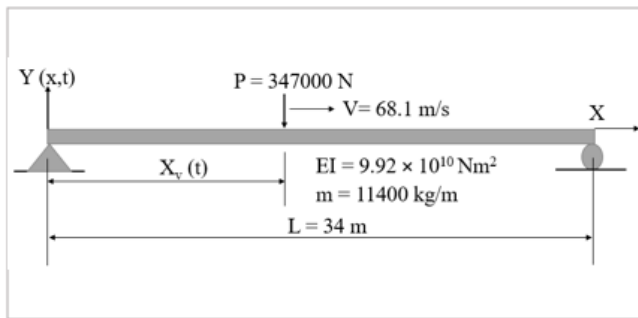


Figure 3. 3 Simply supported bridge subjected to a constant single moving load

The analysis was performed with finite element software SAP 2000 and the results were compared with solution of analytical equation (3.10) in MATLAB code. The vertical mid-span displacement is computed and compared with the output from Finite element model normalized

with respect to maximum static displacement as presented below. Figure 3.3 shows the normalized displacement of mid span of beam with static displacement,  $(U_{dynamic}/U_{static})_{mid}$ , in term of load position on the beam.

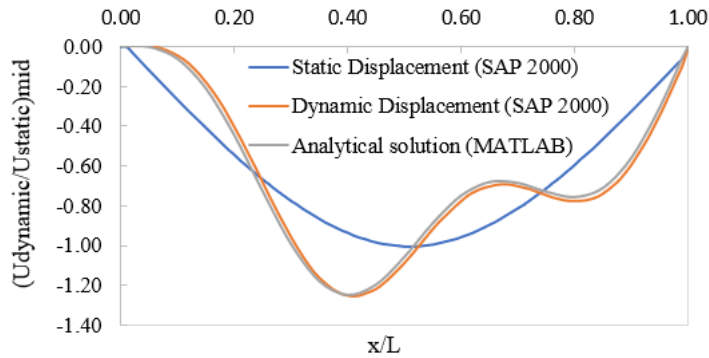


Figure 3. 4 Vertical displacement of simply supported beam subjected to a moving load

The maximum normalized displacement obtained from the analytical calculation in MATLAB (see code in Appendix-A) and FE model in SAP 2000 are particularly matching. In addition to this, the outcome from the current model for the maximum midpoint displacement are also validated with the results in the literatures (Karoumi, n.d.) and (Björklund, n.d.).

The maximum midpoint displacement and acceleration at different speeds of moving load from the FE model are plotted below.

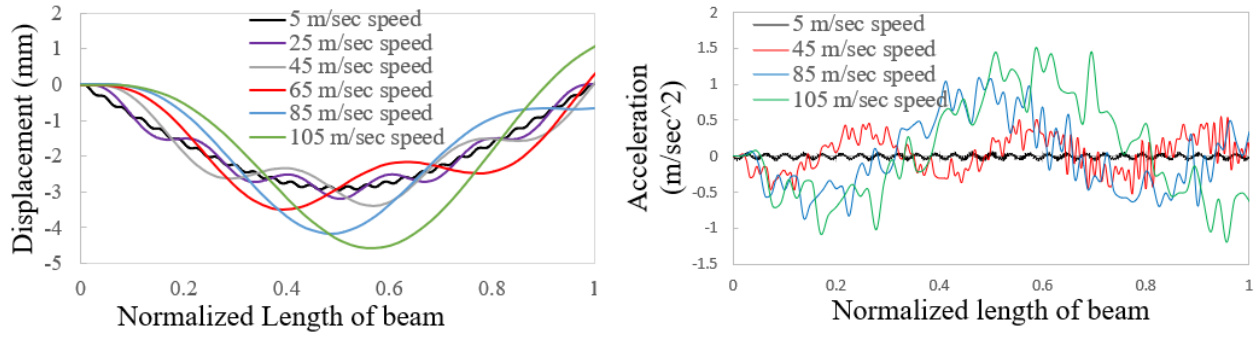


Figure 3. 5: Vertical displacement and acceleration of Simply supported beam subjected to a moving load at different speeds

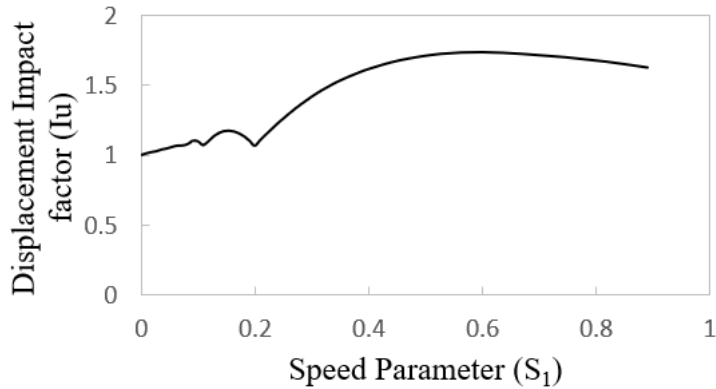


Figure 3. 6 Maximum absolute vertical displacement of Simply supported beam at different speeds

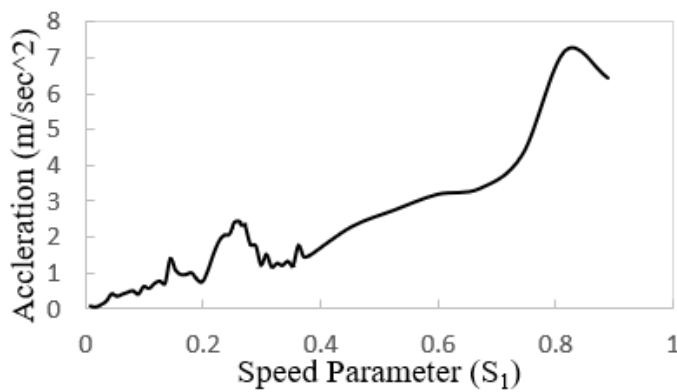


Figure 3. 7 Maximum absolute vertical acceleration of Simply supported beam at different speeds

### 3.2.2 Double Axle Load

The solution for the condition of resonance and cancellation has been numerically investigated and validated. The final element solution of SAP 2000 was utilized to validate the result and response.

Consider simply supported bridge with  $L = 20$  m,  $I = 3.81$  m<sup>4</sup>,  $E = 29.43$  GPa,  $m = 34,088$  kg/m, for which the first frequency of vibration is  $\omega_1 = 44.75$  rad/s. The train has  $N = 5$  cars of identical length  $d = 24$  m. The two-wheels of the car is separated by  $18$  m ( $L_c$ ) and  $L_d = 6$  m. The mass of each wheel assembly is  $M = 22000$  kg, corresponding to  $P = 215.6$  KN. For the current scenario, the maximum static deflection ( $u_s$ ) happens when two-wheel loads  $p$  of interval  $L_d$  are located symmetrically on the beam as shown in Fig. 3.8:

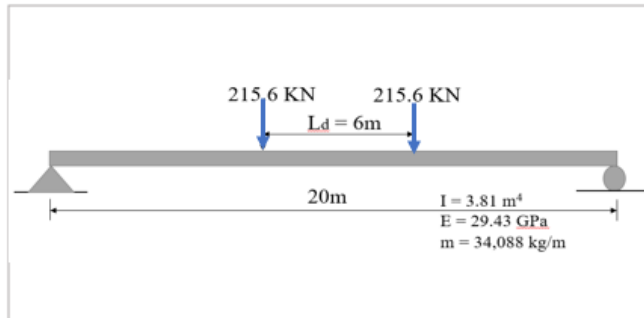


Figure 3. 8: Simply supported bridge subjected to number of moving loads

$$u_s = \frac{pa(3L^2 - 4a^2)}{24EI}$$

Where,  $a = (L - L_d)/2$  for this case.

The speed parameter  $S_1$  is selected by putting  $i = 5$ ,  $S_1 = d/(2iL) = 0.12$ , the resonance speed can be calculated as;

$$v = \frac{S_1 \times \omega_1 \times L}{\pi}$$

$$= 34\text{m/sec}$$

Again, for the condition of cancellation, the speed parameter  $S_1$  is selected to meet the condition.

By putting  $i = 6$ ,  $S_1 = 1/(2i - 1) = 1/11$ , the speed of cancellation is found to be

$$v = \frac{S_1 \times \omega_1 \times L}{\pi} = \frac{44.75 \times 20}{11 \times \pi}$$

$$= 25.9 \text{ m/sec}$$

By modeling the train as a set of wheel loads, the midpoint responses of the beam subjected to the action of the wheel loads moving at the above two speeds have been plotted through the finite element solutions by dividing the beam into 16 elements.

For this case,  $d/L = 1.2$ . So, the points of resonance are at different speed parameter values:  $S_1 = 0.60, 0.30, 0.20, 0.15, 0.12, 0.10$  and the points of cancellation are:  $S_1 = 1.00, 0.33, 0.20, 0.143, 0.111, 0.091$ . Similarly, the speeds of resonance which are calculated as  $v = 171, 85.5, 56.9, 42.75, 34, 28.5$  m/sec and the speeds of cancellation are  $v = 284.89, 94, 57, 40.7, 31.6, 25.9$  m/sec.

The resonance points with  $S_1 = 0.60, 0.15, 0.12$  can generally be observed, while the other resonance points are merely suppressed as they are near the points of cancellation. The first resonance point ( $S_1 = 0.6$ ) should be avoided in practical design for its large value of response.

Similarly, from the FE model in SAP 2000, the resonance points are found plotting the maximum vertical displacements at different speeds of train load model. The resonance speeds

found from the plots are 25, 34 and 43 m/sec which are quite matching with the analytical solution of resonance.

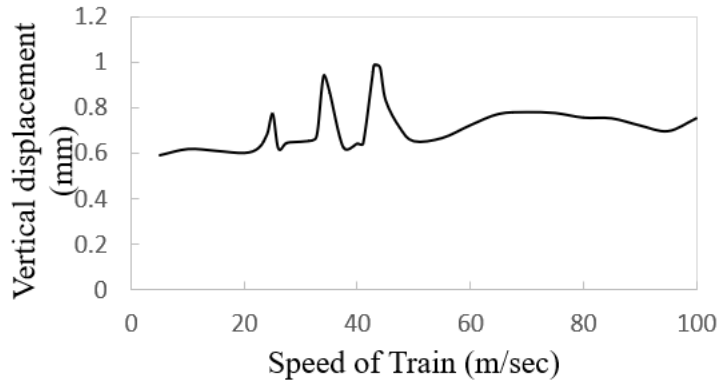


Figure 3. 9 Vertical displacement plot of Simply supported Railroad bridge subjected to train load

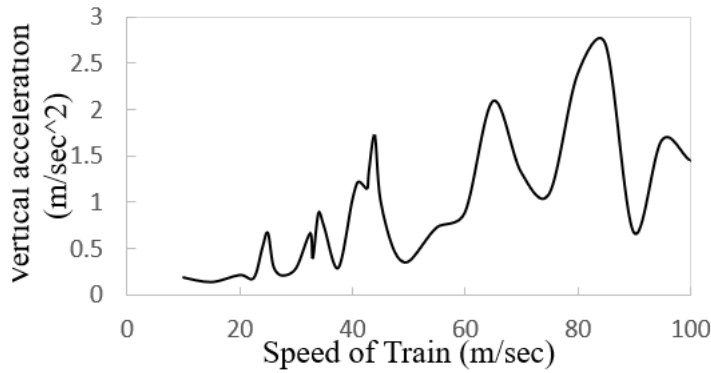


Figure 3. 10 Vertical acceleration plot of Simply supported Railroad bridge subjected to train load

In both the displacement and acceleration plots from FE model, the resonance and cancellation speeds are found at the same points. So, the model in the SAP 2000 is found to be more accurate and valid for a number of moving loads (train load).

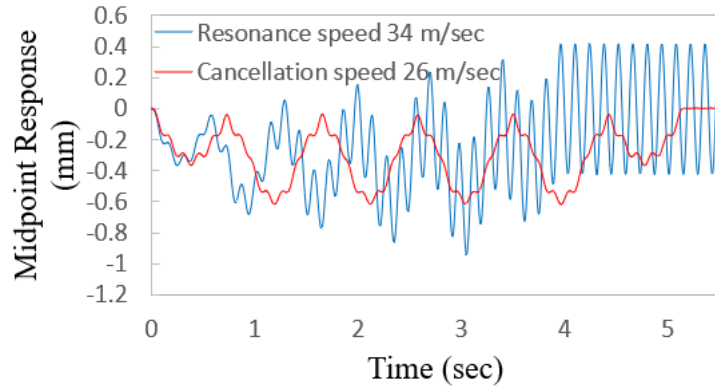


Figure 3. 11 Midpoint response of Simply supported Railroad bridge subjected to a train load at resonance and cancellation speeds in SAP 2000

As shown in figure 3.11, Once the resonance condition happens by number of moving loads, the response of the beam increased as there are more wheel loads passing through the beam and reaches a maximum after passing last wheel load into the beam. FE model in SAP 2000 for the midpoint response in the simply supported beam model at resonance and cancellation speed are particularly matching with the previous literature (Yang et al., 2004).

## CHAPTER IV

### FINITE ELEMENT MODELING OF A RAILROAD BRIDGE

#### **4.1 Devon Railroad Bridge**

The bridge under study is located at Milford, Connecticut and is an open-deck steel truss railroad bridge. It is on the Northeast Rail Corridor between Washington, D.C. and Boston, Massachusetts allocated for higher speed trains. This bridge having seven-span, double track through truss with 325.2m length was built around year 1900 over the Housatonic River. There are two independent parallel bridge structures sharing the abutments and piers. One of the spans near the east abutment with 66.15m length has been taken for this analysis. The tracks are spaced laterally at 3.86 m center-to-center. The rails rest on wood ties that are supported by stringers spaced laterally at 1.98 m on center.

The truss span is 66.15 m long and contains seven panels with stringers connected to floor beams that are spaced 9.45 m on-center longitudinally. A lateral wind bracing system is provided using top and bottom laterals. Truss end-bracings, verticals and top chords are built-up members while midspan diagonals and bottom chords are eye bars of different numbers. Bottom lateral bracing members are single angles, while top lateral bracings are channel sections. The detailed elevation and plan view of the studied truss span is shown in Fig. 4.2 to Fig. 4.4. The

stringers are divided into 14 panels with floor beams longitudinally spaced at 4.725 m. Floor beams are built-up I-sections having a web plate and flanges constructed using angles and cover plates of varying number and thickness. Stringers are rolled, W 36×150, I-beams (Malla et al., 2017).



Figure 4.1 Photograph of Devon railroad bridge, Milford, Connecticut. (Malla et al., 2017)

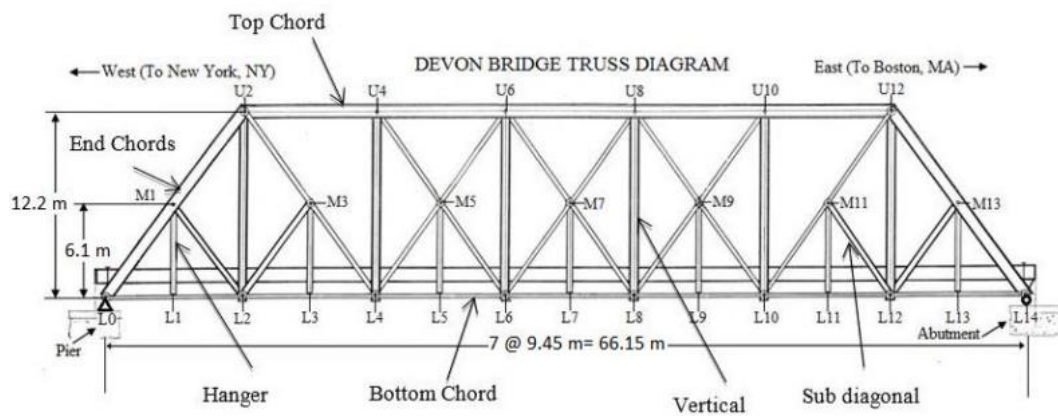


Figure 4.2 Arrangement of principle members of Devon bridge (Baniya et al., 2015)

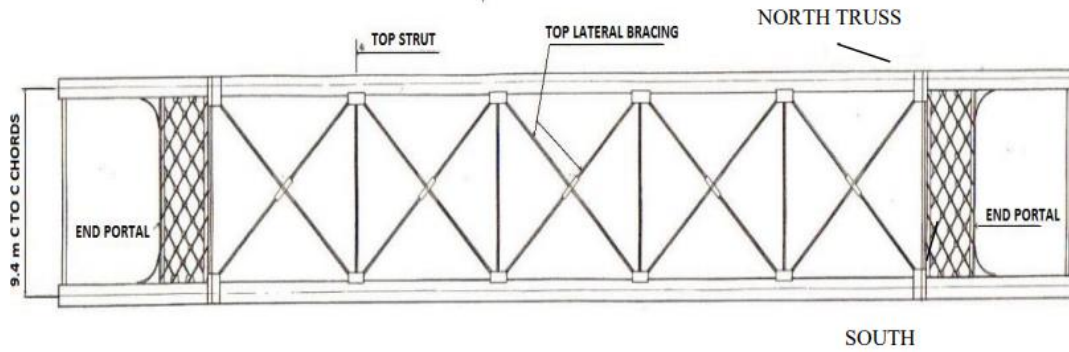


Figure 4.3: Top Chord plan (Baniya et al., 2015)

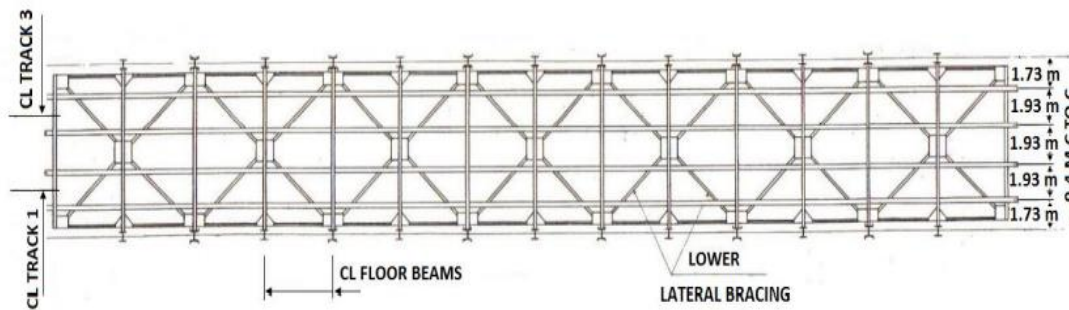


Figure 4.4: Bottom chord plan (Baniya et al., 2015)

## 4.2. Train Loading

The approach of modeling trains is very similar to the number of vehicle systems. The wheels and the track kept in contact, neglecting the influence of mass inertia. There is no option to model the train as a moving mass system in SAP 2000 so the moving load analysis can only be solved for moving constant forces. For this study, Amtrak Acela train has been considered. The configuration of axle load and spacing for this train is considered as per Figure 4.5.

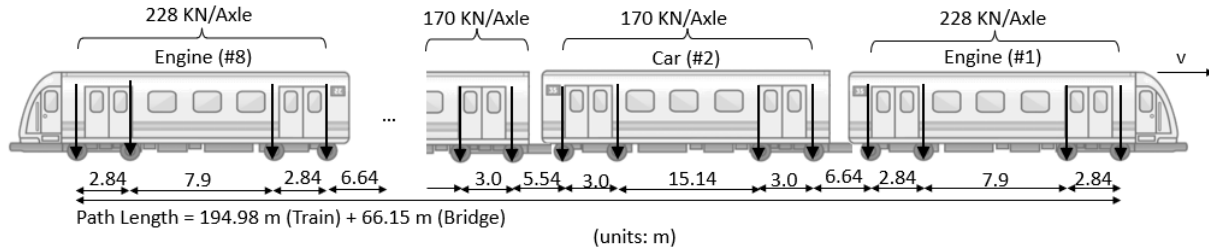


Figure 4.5: Configuration of loading from Amtrak Acela Train

Amtrak Acela train and axle loads have been simulated in SAP 2000 for finite element modeling.

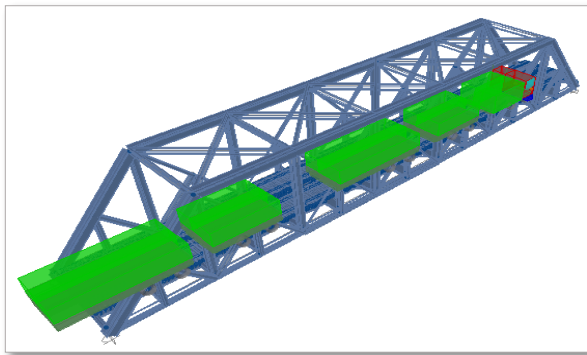


Figure 4.6: 3D model of Amtrak Acela train and axle loads in SAP 2000

### 4.3. Finite Element Model in SAP2000

A 3D numerical model of the Devon railroad bridge is developed using the FE software SAP2000. In the analysis, only the superstructure members of bridge with track system of rails are considered whereas the substructure components such as abutment, column and bearings are not included. The track system of rail sits on the stringers. Loadings from the train system is directly transferred to the rail and subsequently to the stringers and cross girders. The track consists of two rails that are modeled as linear beam elements. Vertical connections between

stringers, fasteners and rails are modeled by rigid links. Two sets of guard rails for each track are considered for modeling. End support of the bridge at the West end was modelled as hinge in which the translations in all the three directions are restrained whereas the support at the East side was modelled as a roller in which the translation in longitudinal direction is released but restrained the translations in two other directions. For the simplification of complex steel truss railroad bridge without compromising the accuracy of result, it is assumed that all the main members of bridge are joined together at the intersection of their centerlines that pass through the centroid of their cross sections. The centerlines of rails, guardrails, and sleepers are also assumed to be joined at the intersection of their centerlines. These are placed at the top of the stringers i.e., 17.5 inches above the centerline of stringers. A rigid element is used to connect them.

The geometry and section properties of the bridge are considered as per the actual drawings and modeled in section designer of FE software.

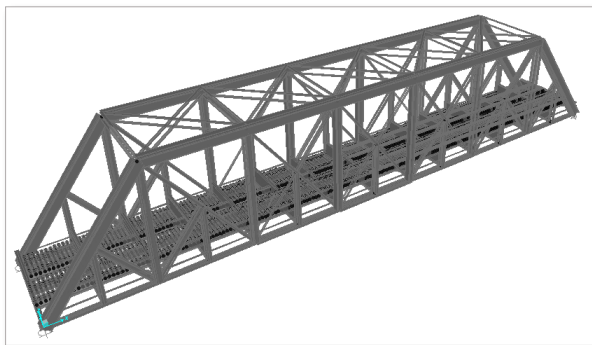


Figure 4.7: 3D model of Devon Steel truss bridge in SAP 2000

For finite element modeling, different members as per the actual bridge condition are considered to be axial and bending members as segregated in the table below.

Table 4. 1 : Axial and Bending members in the Devon railroad bridge.

S.N	Bending members	Axial members
1.	Floor beams	1. Bottom chords (eye bars)
2.	Stringers	2. Top horizontal member
3.	Sleepers	3. Top cross bracing
4.	Rails	4. Diagonals
5.	Vertical members	5. Bottom cross bracing
6.	End slope members	
7.	Hangers	
8.	Top chords	

#### 4.4. Model Validation

The field test data of Devon Bridge that was performed with accelerometers and linear variable differential transducers (LVDT) during the passage of trains are used for validation (Malla et al., 2017). The modal analysis of the Bridge was performed to obtain the mode shapes and natural frequencies of vibration. There are several elements in a truss bridge which create local modes of vibrations. The model is correlated and validated with the experimental data. Natural frequencies of the bridge model obtained are quite close to the data from the field experiment.

Table 4. 2: Natural frequencies of different modes from FE model and field study

Mode Number (Global)	Natural Frequency (Hz)	
	FE model	Field data (Malla et al., 2017)
First lateral mode (Mode 1)	1.6	1.6
Second lateral mode (Mode 2)	2.5	3.3
First vertical mode (Mode 4)	4.4	4.6

Table 4.2 compares the natural frequencies of modes 1, 2, and 4 of FE model with those computed by processing the acceleration data collected on the Devon railroad bridge during a field study performed by Malla et. al. (2017). It is seen that there is a small difference between the natural frequencies of FE model and those computed from the field testing.

#### 4.5. Natural Frequencies and Mode Shapes

The modal analysis of the bridge was performed to obtain the mode shapes and natural frequencies of vibration. A total of 50 mode shapes and frequencies were considered in the FE model. The global natural frequencies and mode shapes obtained from the FE model are considerably close to the field experimental data. The major mode shapes are captured from the model and presented below.

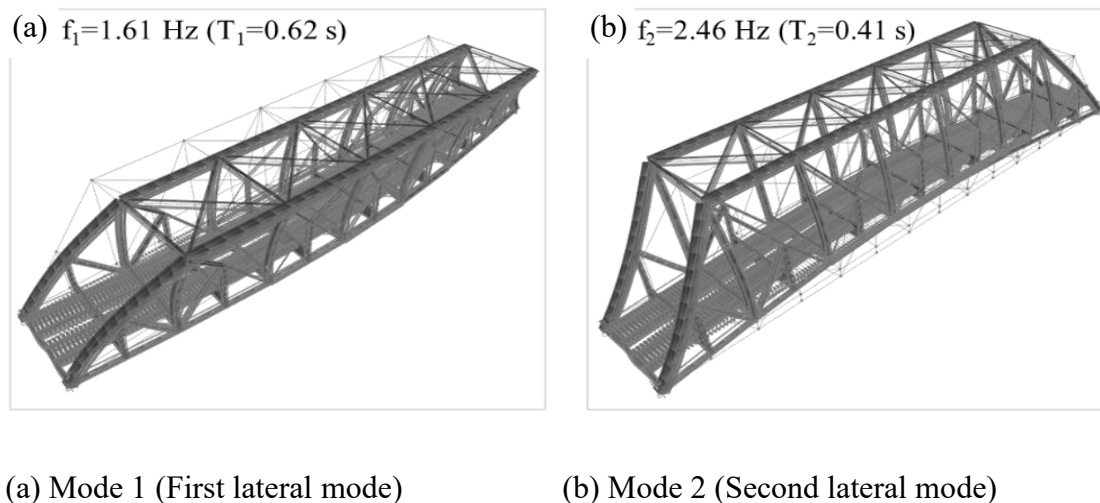
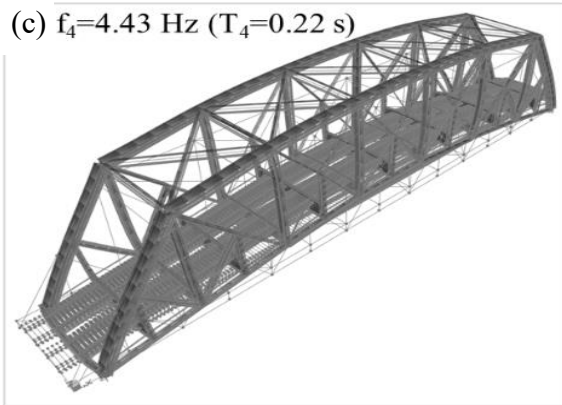


Figure 4.8 Mode shapes of the bridge resulted from the FE model.



(c) Mode 4 (First vertical mode)

Figure 4.8, contd.

#### 4.6. Transient Time History Analysis

The transient time history analysis of the finite element model was performed to obtain the acceleration response at different damage cases. For this analysis, Amtrak Acela train was moved in the track at North side with various speeds. Higher speed of moving trains excites larger frequencies of vibrations in the calculation of response of bridge.

The influence of damage can be seen as acceleration sparks in the measured acceleration signals. The vertical acceleration has been utilized as it is more sensitive to the damage and loss of stiffness of deck members.

##### 4.6.1. Sensitivity Analysis: Time Step

Selection of a proper time step is very critical to achieve precise results in dynamic time history analysis of bridges especially when there is an impact load. In this sensitivity analysis, the optimum time step has been analyzed considering impact load as well as the efficient computational time of FE model.

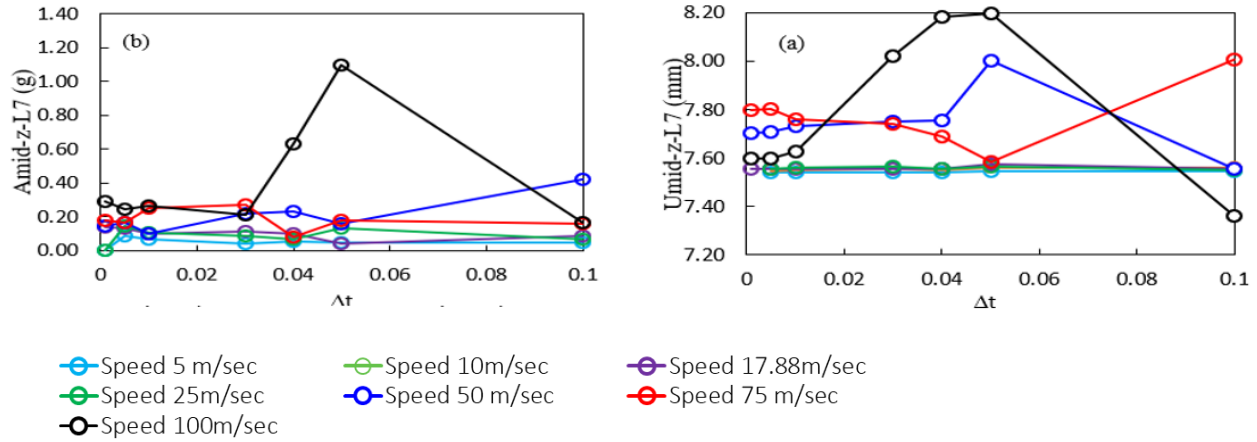


Figure 4.9: Sensitivity analysis for optimum time step

From the plots of vertical acceleration and displacement shown in figure 4.9, the optimum time-step for the analysis was found to be 0.01 sec which can capture the impact considering the efficient computational time.

#### 4.6.2. Sensitivity Analysis: Damping Ratio

Sensitivity Analysis – Damping Ratio

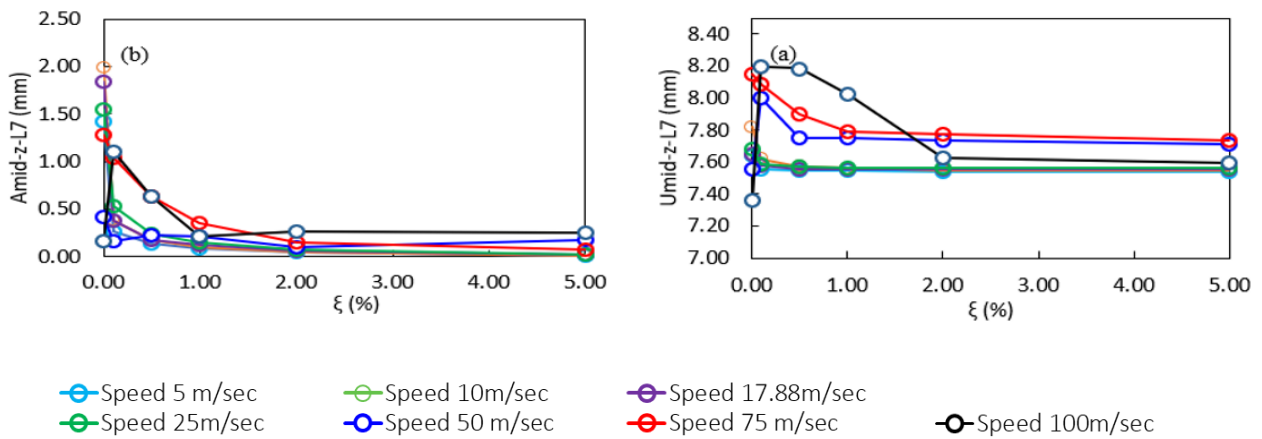


Figure 4.10: Sensitivity analysis for damping ratio

Based on the field test results (Malla et al., 2017), the following damping values for different modes are obtained.

Table 4. 3 Damping Ratio for different Modes of the Bridge

Modes	Damping Ratio (%)
First Lateral Mode	3.84
First Vertical Mode	2.17

Comparing the sensitivity analysis with the field test results, it was concluded that the damping ratio values from the field test can be used for further analysis. Accordingly, the same values were used for finite element modeling of the railroad bridge.

#### 4.7. Resonance Speed

The response of bridge under a moving train load is complicated because the frequency contents in the excitation involve not only characteristics from a moving load but also repeated load pulses from consecutive carriages. There are mainly two concerning parts; one is the variation of the natural frequencies of the bridge during the passage of train loads called driving frequency and the another is the frequency contents in the trainload excitation and their effect in the bridge response called dominant frequency.

Critical speed is the condition under which a bridge reaches the maximum response when subjected to a single moving load. However, when multiple loads are involved, the frequency of the excitation will feature the apparent dominant frequencies that associate with time intervals between consecutive loads, in addition to the driving frequencies. Consequently, the resonance is expected to exhibit a different character beyond the context of the critical speed. It has been

generally understood that when a specific dominant frequency from the multiple loads coincides with one of the first few bridges natural frequencies, especially the first bridge natural frequency, resonance to a certain degree would occur.

The response of the bridge under a series of moving loads at the resonance speed will always tend to increase. It is the rate of increase between the consecutive moving loads that determines the severity of the resonance effect (Mao & Lu, 2013).

The assessment of the bridge resonance under the excitation of Amtrak Acela train loads, without considering the mass has been obtained and demonstrated as below.

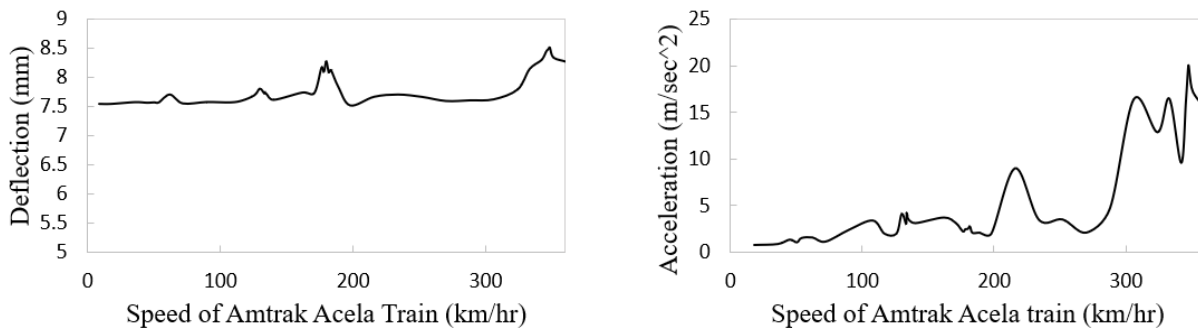


Figure 4.11: Midspan vertical deflection and acceleration vs moving speed of Amtrak Acela Train

Figure 4.11 shows the deflection and acceleration at midspan of the bridge, it can be clearly seen that the intense resonance is excited at around 180 km/hr (50 m/s), whereas the next peaks appear at around 62 km/hr (17.3 m/sec) and 130 km/hr (36 m/s).

## CHAPTER V

### DAMAGE QUANTIFICATION

#### 5.1. Damage to the Stringer-to-Girder Joints

Damage may appear on the deck of a steel railroad bridge due to different factors including the impact load of train wheels and its effects on response of the deck members to fatigue load that can result in either strength loss or stiffness loss. The structural integrity of open deck railroad bridges depends mostly on the condition of the steel girders and stringers that form the framework of the bridge. Corrosion, fatigue load and excessive weight can all cause damage to these components, leading to potential safety hazards. In finite element modeling, this problem can be demonstrated by reducing the rotational stiffness of the affected zone as reported in various literatures (Rageh et al., 2020) (Al-Emrani, 2005). Change in the rotational stiffness of Stringer-to-Girder (StG) joint can represent real damage in the railroad bridges. Figure 5.1 shows an example of a such a joint with the possibility of cracks.



Figure 5. 1 example of Stringer-to-Girder joint with possibility of cracks (Rageh, 2020)

Figure 5.2. shows the details of the joint including stringer, floor beam (cross girder), angles, and the pattern of cracks due to fatigue.

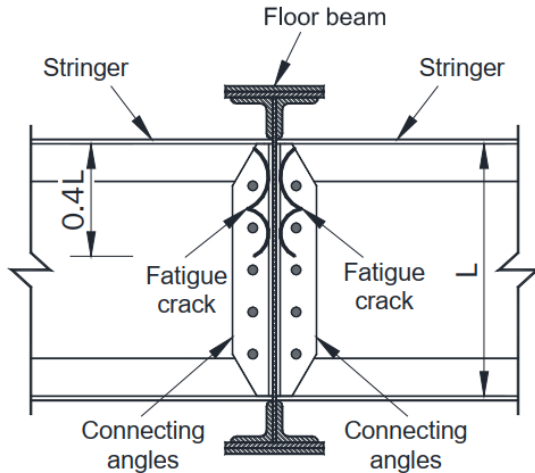


Figure 5. 2 Details of a Joint including fatigue cracks(Rageh et al., 2020)

Figure 5.3. shows how the development of cracks changes the rotational stiffness of the stringer. Gradual reduction in the rotational stiffness of the connections was observed because of crack development in the connection angles. This reduction was accompanied by a decrease in the amount of restrained stringer-end rotation and the corresponding forces acting on the connection. Consequently, there was a significant impact on the propagation rate of the cracks, leading to a noticeable decrease. The increase in bending stress in the mid-span of the stringers during different stages of crack propagation could be monitored, which clearly demonstrated this behavior.

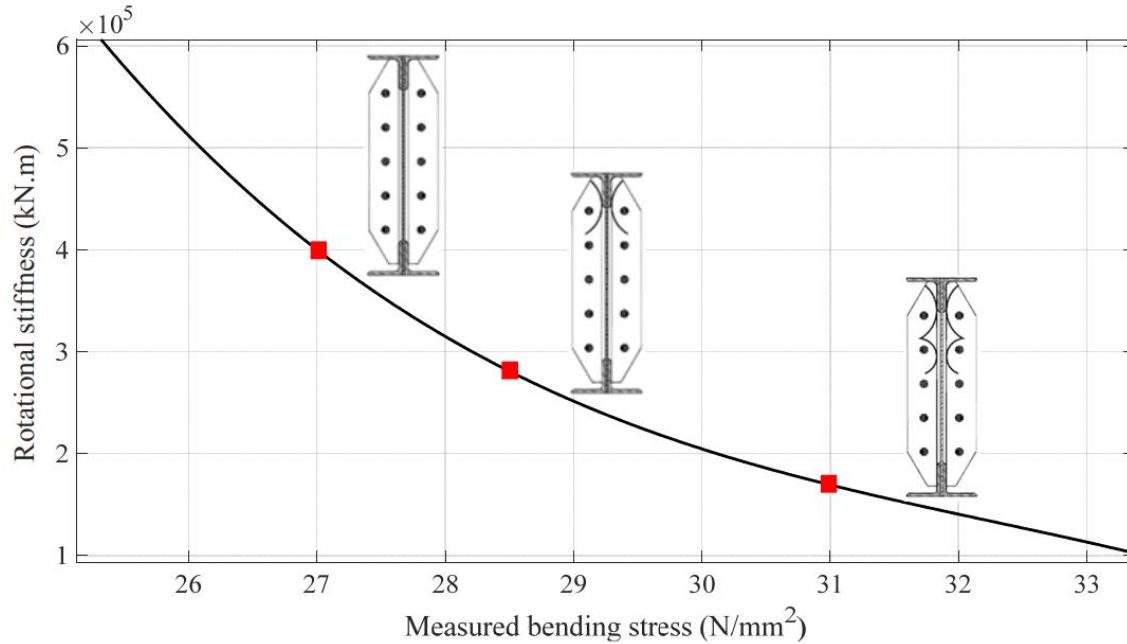


Figure 5. 3: Change of rotational stiffness with the progress of crack in the Stringer-to-Girder joint (Rageh et al., 2020)

The joint considered for the damage modeling includes only the middle panel of deck as shown in Figure 5.4 below. For this study, different scenarios are considered for modeling damage in the bridge. Change in rotational stiffness of the stringers with the change in Moment of Inertia of the joint section because of damage is given as:  $I_D = \alpha I_H$ , with different values of  $\alpha=0.01$  (or  $\alpha \approx 0$  as highly damaged case),  $\alpha=0.50$  (low damage), and  $\alpha=1.0$  (no damage or healthy case). Where,  $I_D$  is the moment of inertia of the damaged stringer section and  $I_H$  is the moment of inertia of the healthy stringer section. Note that the rotational stiffness of stringers at the stringer-to-girder joints is described by  $K_\theta = \mu EI/L^3$  where  $L$  is the length of the stringer and  $\mu$  is a constant that depends on the stiffness of both the stringer and cross girder (or support condition).

Healthy and damage cases are considered for the dynamic analysis of the railroad bridge to detect damage from the acceleration signal measured by sensors deployed around the damage zone (See Figure 5.4). In this study, total 12 number of sensors are installed in different locations of the bridge model to measure acceleration signals. The change in responses for different damage cases from all the sensors are used to identify damage in the bridge through different features.

The vertical acceleration of deck is very sensitive to the passage of trains and usually it has a significantly higher magnitude than accelerations in other directions. For this reason, vertical acceleration is more capable to detect the damage and loss of stiffness of Stringer-to-Girder joint.

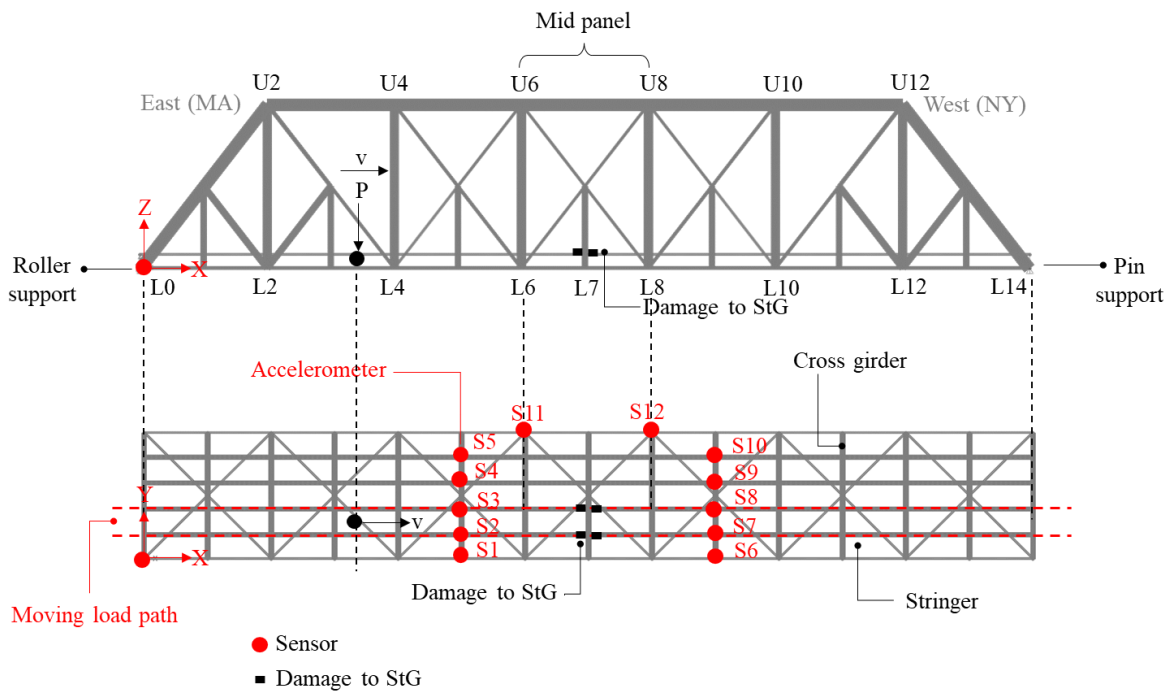


Figure 5. 4: Devon railroad bridge elevation and plan with location of sensors and damage

## 5.2. Defect in the Rail

Rail is a major component of the railroad system as it performs two critical functions, namely, transferring the wheel loads to the track bed and guiding the train cars along the track. However, due to its constant exposure to the moving load of the train, the rail is susceptible to rolling contact fatigue and wear. This gradual wear and tear can eventually cause the rail to break and lead to train derailment. If such an accident occurs on a railroad bridge, it can cause severe damage to the structure. For instance, the Tempe Town Lake steel railroad bridge suffered structural failure in July 2020, costing \$11 million to repair. Thus, early detection of any defects in the railroad bridge can prevent catastrophic accidents and irreversible damage.

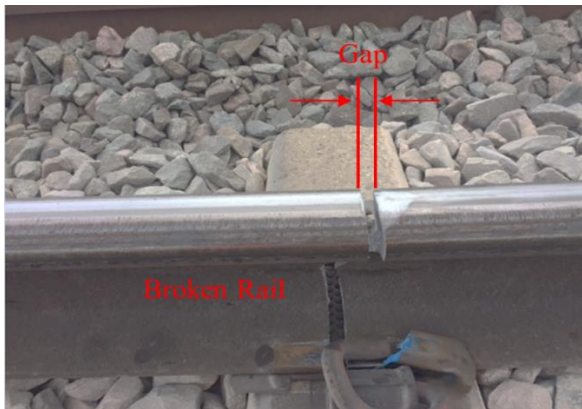


Figure 5. 5 Example of a broken rail

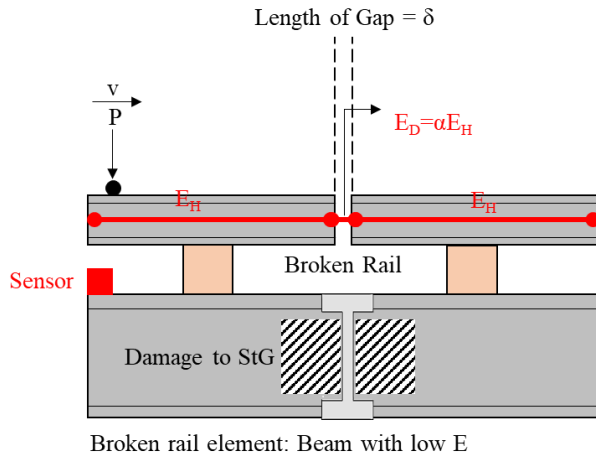


Figure 5.6 Modeling of a broken rail in the FE model.

For this case, the damage is considered as broken rail. This damage is considered in the mid part of rail-bridge that has been modeled by considering the reduced value of modulus of elasticity of rail element as:  $E_D = \alpha E_H$  as shown in Figure 5.6.

Figure 5.7 shows the variation of the displacement and acceleration of a joint very close to the damage zone (Joint No. 1663 at the edge of gap in Figure 5.8) with the size of gap of the broken rail denoted by  $\delta$  in cm. A sensitivity analysis is performed to see how the gap size (or  $\delta$ ) changes the response of the FE model (see figure 5.7). It is seen that the change in the gap from 0.5 cm to 2.0 cm does not really change these two responses. In this study, it is assumed that the size of gap is 5 mm.

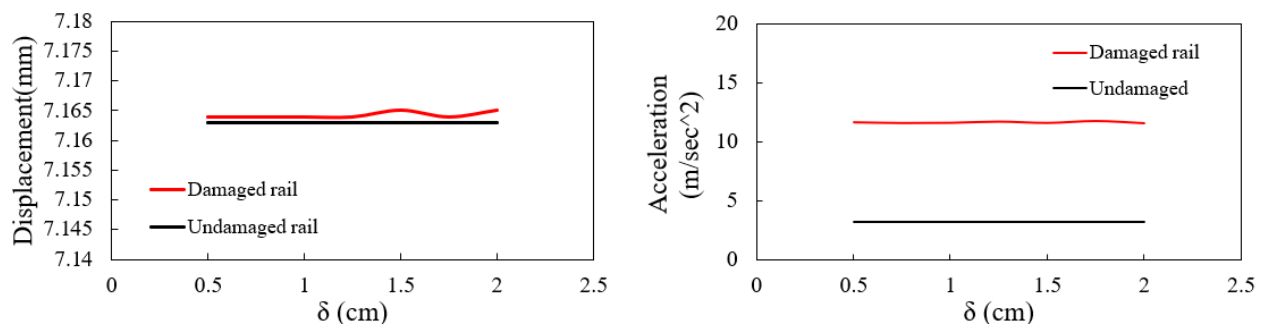


Figure 5.7 Sensitivity Analysis for length of Crack in rail with the variation of displacement and acceleration at joint 1663.

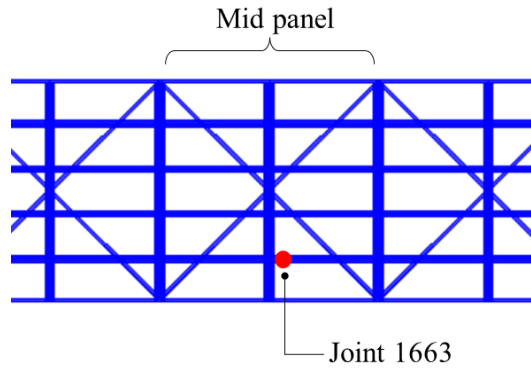


Figure 5.8 Joint 1663 in the stringer below the edge of gap in the rail (broken rail)

### 5.3. Vibration Features

In this study, we quantify damage by calculating the vibration features of acceleration signals measured by the accelerometers S1, S2, ..., S12.

#### 5.3.1. Time Domain Features

When damage occurs, the stiffness of the bridge structure around the damage area changes, which can cause impulse in the response of the bridge. This impulse may further result in the variation of the collected acceleration signals changing amplitudes and distributions of these time-domain features. Below are some common statistical features in the time domain considered in this study for the extraction of features from the acceleration signal to detect the level of damage (Lei, 2016).

Table 5.1 Statistical Features in the Time Domain used for the extraction of features.

T <sub>1</sub>	$X_m = \frac{1}{N} \sum_{n=1}^N x_n$	Mean value
T <sub>2</sub>	$X_{rms} = \sqrt{\frac{1}{N} \sum_{n=1}^N x_n^2}$	Root Mean Square
T <sub>3</sub>	$X_{sd} = \sqrt{\frac{1}{N-1} \sum_{n=1}^N (x_n - X_m)^2}$	Standard Deviation
T <sub>4</sub>	$X_{skew} = \frac{1}{N-1} \sum_{n=1}^N \left( \frac{x_n - X_m}{X_{sd}} \right)^3$	Skewness
T <sub>5</sub>	$X_{kurt} = \frac{1}{N-1} \sum_{n=1}^N \left( \frac{x_n - X_m}{X_{sd}} \right)^4$	Kurtosis
T <sub>6</sub>	$X_{peak} = \max( x_n )$	Peak
T <sub>7</sub>	$X_{crest} = \frac{X_{peak}}{X_{rms}}$	Crest

In Table 5.1, the signal's average is denoted by  $X_m$ , and its standard deviation is represented by  $X_{sd}$ . The root mean square of the signal is denoted by  $X_{rms}$ , and the signal's peak by  $X_{peak}$ , which reflects its vibration amplitude and energy. These four features can distinctly reflect the degree of damage in a structure when it becomes more severe. However, they are not sensitive enough to detect mild damage. When mild damage occurs, Skewness ( $X_{skewness}$ ), kurtosis value ( $X_{kurtosis}$ ), and crest factor ( $X_{crest}$ ) can be used to represent the time series distribution of the signals in the time domain.

It should be noted that the kurtosis and crest values are specifically used to measure the impulse existing in vibration signals induced by not only the moving wheel load but also the damage in both StG and rail (Lei, 2016).

The kurtosis value and crest factor are reliable indicators for detecting early damages and are strong at varying operating conditions. They are effective in indicating the spikiness of sharp impulses generated by defects in the bearing mating surfaces. It is worth noting that the kurtosis value is highly sensitive to early damage, and its value can gradually increase as the degree of

severity increases. However, for more severe damage, the kurtosis value unexpectedly decreases, making it unsuitable as an indicator for such cases.

In the formulas described in Table 5.1,  $x(n)$  is a signal (acceleration) series for  $n = 1, 2, \dots, N$  and  $N$  is the number of data points.

### 5.3.2. Time-Frequency Domain Features: Hilbert-Huang Transform

The Hilbert-Huang transform (HHT) is a powerful tool for performing time-frequency analysis of non-stationary and non-linear signals to unearth the complex implications hidden in the time series data that otherwise cannot be revealed by traditional data analysis such as Fourier Transform (FT) (Huang & Wu, 2008). The acceleration signals recorded by accelerometers on a railroad bridge when a train passes by are examples of non-stationary and non-linear time series data that can be analyzed by HHT to describe them in term of time, frequency, and energy at the same time.

The HHT of acceleration signal  $\ddot{u}(t)$  is computed in two steps: (1) the empirical mode decomposition (EMD) and (2) the Hilbert spectrum (HS). In the first step, the acceleration signal  $\ddot{u}(t)$  is decomposed into a finite number of intrinsic mode functions (IMFs) as follows,

$$u(t) = \sum_{i=1}^M x_i(t) + x_0(t) \quad (5.1)$$

Where,  $\ddot{x}_i(t)$  is the  $i$ -th IMF signal and  $\ddot{x}_0(t)$  is the residue. Each IMF signal must satisfy the following conditions (Roveri & Carcaterra, 2012): (1) the number of extrema and the number of zero-crossings in the signal must be either equal or differ at most by one, and (2) the mean value of envelope defined by the local maxima and the envelope defined by the local minima is zero. These conditions ensure that each IMF signal is mono-component and has a well-behaved Hilbert Transform (HT), that is, at any time the signal must have a single positive instantaneous

frequency defined by the derivative of its phase function. In the second step, the analytic signal  $\tilde{z}_i(t)$  is defined for the  $i$ -th IMF signal as follows,

$$z_i(t) = x_i(t) + jy_i(t) \quad (5.2)$$

Where,  $j$  is the imaginary unit and  $y_i(t)$  is the HT of  $i$ -th IMF signal that is defined as (Huang & Wu, 2008),

$$y_i(t) = H\{x_i(t)\} = \frac{1}{\pi} \int_0^{t_N} \frac{x_i(\tau)}{t - \tau} d\tau \quad (5.3)$$

The analytic signal  $\tilde{z}_i(t)$  is a complex-valued function that can be described in the following polar form,

$$z_i(t) = a_i(t)\exp [j\phi_i(t)] \quad (5.4)$$

Where,  $a_i(t)$  and  $\phi_i(t)$  are the instantaneous amplitude and phase of signal that are given by,

$$a_i(t) = \sqrt{x_i^2(t) + y_i^2(t)} \quad (5.5)$$

$$\phi_i(t) = \tan^{-1} \left( \frac{y_i(t)}{x_i(t)} \right)$$

The instantaneous angular (circular) frequency of  $i$ -th IMF signal can be calculated by taking the first derivative of  $\phi_i(t)$ ,

$$\omega_i(t) = \frac{d\phi_i(t)}{dt} \quad (5.6)$$

The instantaneous energy of  $i$ -th IMF signal describing its intensity is given by,

$$E_i(t) = |a_i(t)|^2 \quad (5.7)$$

Finally, the time-frequency distribution of instantaneous amplitude in the 3D space  $\{t, \omega_i, a_i\}$  is called Hilbert spectrum (HS) for  $i$ -th IMF that is denoted by  $H_i(\omega, t)$ . The HS of original acceleration signal  $\ddot{u}(t)$  is defined as,

$$H(\omega, t) = \sum_{i=1}^M H_i(\omega, t) \quad (5.8)$$

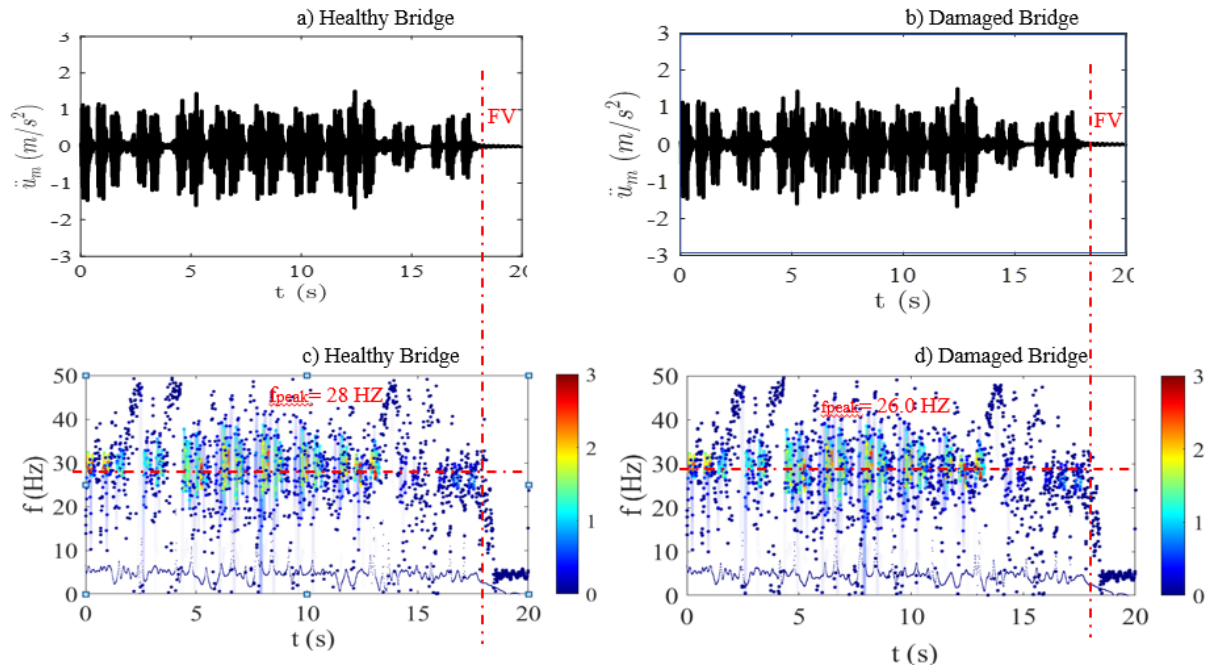


Figure 5. 9 Hilbert spectral analysis of the acceleration signal recorded by S2 for train speed of 15m/sec speed a) healthy rail healthy bridge acceleration b) healthy rail damaged bridge acceleration c) Healthy rail and healthy bridge Hilbert spectrum d) healthy rail damaged bridge Hilbert spectrum e) Rail defect highly damaged bridge acceleration f) Rail defect highly damaged bridge Hilbert spectrum

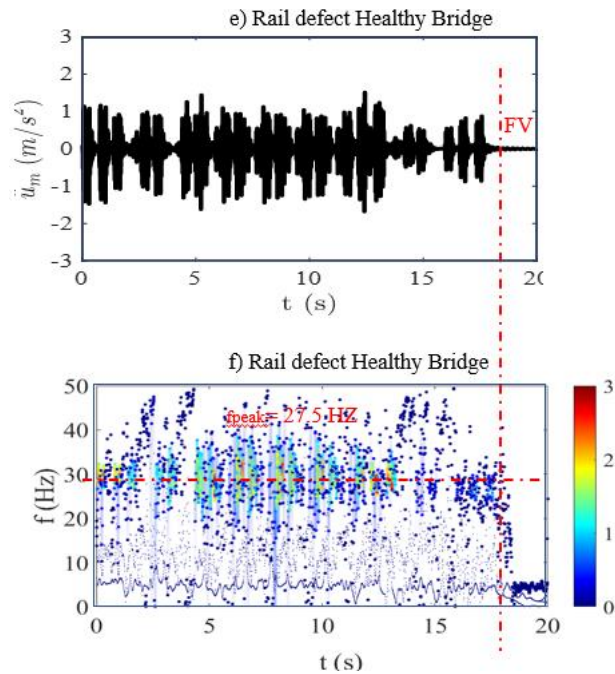


Figure 5. 9, contd.

### 5.3.3. Feature Scaling (Normalization)

The feature properties of the data will vary depending on the source of the data. Data normalization is an important pre-processing technique that involves either rescaling or converting data to ensure that each feature has an equal contribution. Normalizing features is an effective technique that limits the values of all features to predefined ranges. This helps to enhance the quality of data and consequently, the performance of machine learning algorithms. Normalization addresses two significant issues of data that impede the learning process of machine learning algorithms, namely the existence of dominant features and outliers. Various techniques are employed to adjust the data to a specific range using statistical parameters derived

from the original data. It is crucial to select the appropriate normalization method and range since normalization can alter the data's structure and can impact the results of multivariate analysis and calibration utilized in pattern recognition (Singh & Singh, 2020).

In this study, the dataset with  $f$  number of features is normalized and represented by damage indices (DI) as below.

$$DI_i = 1 - \frac{(X_i)_D}{(X_i)_H} \times 100 \quad (5.9)$$

Where,  $i=m, rms, sd, kurtosis, skewness, peak, crest$  (time domain features)

The damage at the joint between stringer to cross girder in the middle panel is quantified and normalized by time domain features  $DI_m, DI_{rms}, DI_{sd}, DI_{kurtosis}, DI_{skewness}, DI_{peak}$ , and  $DI_{crest}$  and time-frequency domain features  $DI_E$  and  $DI_\phi$  describing the changes in the energy and phase of recorded acceleration signals.  $DI > 0$  indicates the presence of damage in the StG of a deck, and  $DI = 0$  indicates no damage. The energy damage index  $DI_E$  is defined as,

$$DI_E = 1 - \frac{(S_E)_D}{(S_E)_H} \times 100 \quad (5.10)$$

Where  $S_E$  is the area below the energy function  $E(t)$  that is defined as,

$$E(t) = \int_0^{\omega_n} H^2(\omega, t) d\omega \quad (5.11)$$

The phase damage index  $DI_\phi$  is defined as,

$$DI_\phi = \left| 1 - \frac{(\bar{\Phi})_D}{(\bar{\Phi})_H} \right| \times 100 \quad (5.12)$$

Where,  $\bar{\Phi}$  is the average of instantaneous phase of recorded acceleration signal taken over time and of IMFs which is defined as:

$$\bar{\Phi} = \frac{1}{NM} \sum_{i=1}^M \sum_{n=1}^N \phi_i(t_n) \quad (5.13)$$

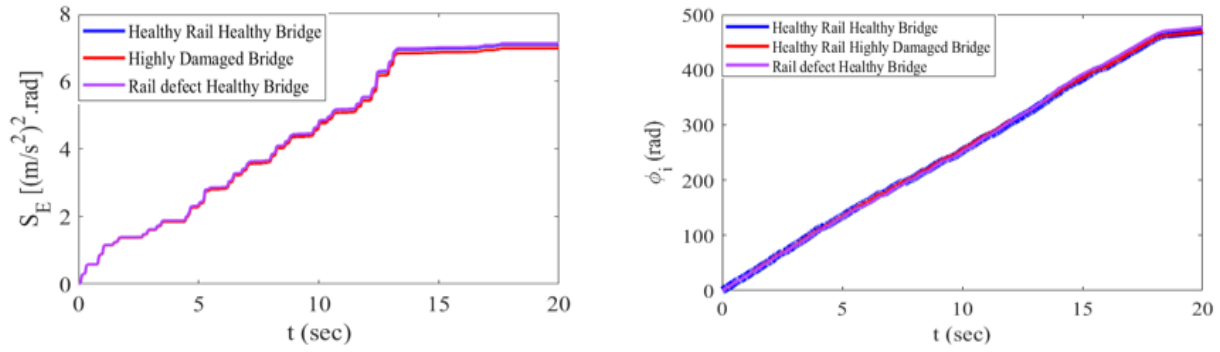


Figure 5. 10 Energy and Instantaneous phase of recorded acceleration signals for S2 sensor location in the healthy rail and bridge compared to highly damaged bridge at 15 m/sec speed

## CHAPTER VI

### DAMAGE CLASSIFICATION

#### 6.1. Machine Learning Classifiers

##### 6.1.1. Support Vector Machine (SVM)

SVM classifier was first introduced by Vapnik in the 1960s on statistical learning theory and later improvised in the 1990s. SVM is one of the effective supervised machine learning methods in data classification as well as text classification that has become extremely popular these days due to its particularly efficient results. In terms of runtime, this is the fastest algorithm and has great accuracy. This classification is effective in high dimensional spaces (e.g., vibration features).

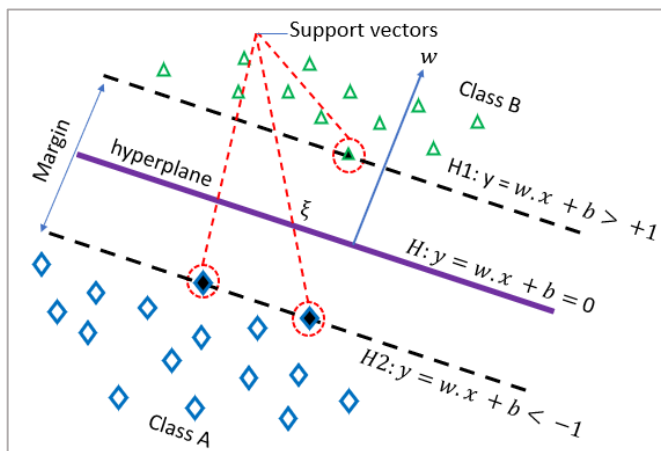


Figure 6.1. Graphical representation of SVM classification with optimal and marginal hyperplanes

The main idea behind SVM is to take the data from a lower dimension to a higher dimensional space to separate them easily. SVM is a discriminative classifier that is properly engineered by separative hyperplane. It is a representation of examples as points in space that are mapped so that the points of different categories are separated by a gap as wide as possible. In addition to this, an SVM can also perform non-linear classifications. The distance is maximized from the hyperplane to the closest data points called margin.

The formulation of a basic SVM has been constructed from a simple linear maximum margin classifier as per below (Rojas & Nandi, 2006):

For the datasets:  $(x_1, y_1), (x_2, y_2) \dots (x_n, y_n)$

Where,  $x_i$  is a  $d$ -dimensional input vector in  $R^d$  and  $y_i$  is the class label associated with  $x_i$ ,

For every  $i = 1, 2, \dots, n$ ; finding classifier having decision function  $f(x)$ , such that  $f(x) = y$  for each dataset.

Let us consider the labels be  $y_i \in \{+1, -1\}$  for two possible classes A and B. The objective of the classifier is to define a boundary between the datasets with both labels (+ and -). The boundary is a hyperplane where all the datasets satisfy (Rojas & Nandi, 2006),

$$f(x) = \text{sign}(w \cdot x + b) \quad (6.1)$$

Where,  $w \in R^d$  is a normal vector to the boundary and  $b$  is the distance from the boundary to the origin of reference. The best boundary can be formulated with all the three parallel hyperplanes shown in Figure 6.1 accordingly,

$$H: y = w \cdot x + b = 0 \quad (6.2)$$

$$H1: y = w \cdot x + b = +1$$

$$H2: y = w \cdot x + b = -1$$

The normal distance between hyperplane H1 and hyperplane H2 is a margin with a magnitude of  $2/\|w\|^2$ . The classifier with the largest margin will show the best generalization for data points that were not in the dataset. Thus, finding the best hyperplane is changed into a linearly constrained optimization problem.

To maximize the margin between hyperplanes H1 and H2, subject to the restriction,

$$y_i(w \cdot x_i + b) \geq 1 \quad (6.3)$$

The optimization problem is a quadratic problem in  $(w,b)$ , which can be better formulated in terms of Lagrange multipliers,

$$L(w, b, \vec{\alpha}) \equiv \frac{\|w\|^2}{2} - \sum_{i=1}^n \alpha_i y_i (w \cdot x_i + b) + \sum_{i=1}^n \alpha_i \quad (6.4)$$

The minimization of the term with respect to  $w$  and  $b$ , while requiring the derivatives of  $L$  with respect to  $\alpha$  to vanish. The  $\alpha_i$  in equation (6.4) are the Lagrange multipliers, and it is required that  $\alpha_i \geq 0, i = 1, 2, \dots, n$ .

Equation (6.4) is a convex quadratic problem with an equivalent Wolfe's dual formulation that can be solved instead, with the benefit that  $w$  and  $b$  vanish. The dual comprises in maximizing  $L$  with respect to  $\alpha$  while requires its gradient with respect to  $w$  and  $b$  to vanish.

This gives the two conditions.

$$w = \sum_i \alpha_i y_i x_i \quad \text{and} \quad \sum_i \alpha_i y_i = 0 \quad (6.5)$$

After substituting equation (6.5) into equation (6.4), it gives the Lagrangian dual.

$$L_{\text{Dual}} \equiv \sum_{i=1}^n \alpha_i - \frac{1}{2} \sum_{ij} \alpha_i \alpha_j y_i y_j x_i \cdot x_j \quad (6.6)$$

This needs to be maximized with respect to  $\alpha$ . After the dual problem is solved for all  $\alpha_i$ ,  $w$  and  $b$  can be obtained; thus.

$$\begin{aligned} f(x) &= \text{sign}(w \cdot x + b) \\ &= \text{sign} \left( \sum_{i=1}^n \alpha_i y_i (x_i \cdot x) + b \right) \end{aligned} \quad (6.7)$$

When the surface separating the two classes is non-linear, the training datasets can be transformed to a higher dimensional space, to make the separation linear in that new space and applied the same process.

Let the transformation over the dataset be  $\phi(\cdot)$  and let  $K(x_i, x_j) = \phi(x_i) \cdot \phi(x_j)$ ;

Equation (6.6) can be rewritten as.

$$L_{\text{Dual,nonlinear}} \equiv \sum_{i=1}^n \alpha_i - \frac{1}{2} \sum_{ij} \alpha_i \alpha_j y_i y_j (K(x_i, x_j)) \quad (6.8)$$

Replace  $x_i, x_j$  by the kernel function  $K(x_i, x_j)$  allows the algorithm to produce an SVM which exists in a high dimensional space. The separation is still linear, though in a different space. An upper limit is required to the constraint imposed on the Lagrange multipliers to allow flawed separation. This limit is a penalty applied to those points which lie in between the surfaces  $H_1$  and  $H_2$ . For the perfect separation case, the penalty is infinite, with no points inside the margin; the penalty  $C$  is given as finite value of:

$$0 \leq \alpha_i \leq C, \quad i = 1, 2, \dots, n \quad (6.9)$$

Equations (6.8) and (6.9) form the objective function for a nonlinear problem that is used in the algorithms for training two-class SVMs. The SVM should be able to classify the data points not included in the training with a certain degree of success. With the same concept of binary classifiers, the multi-class case can be combined. For the  $n$ -class case,  $n$  classifiers are

trained putting one class at a time and grouping the rest as another label. After training, a new point is assigned to that class (Rojas & Nandi, 2006).

In this study, the following SVM algorithms under all SVMs classifier are evaluated to classify the damage cases: (i) Linear SVM (ii) Quadratic SVM (iii) Cubic SVM (iv) Fine Gaussian SVM (v) Medium Gaussian SVM (vi) Coarse Gaussian SVM

### **6.1.2. K-Nearest Neighbor (KNN)**

KNN is a machine learning technique that can be applied to solve classification and regression problems. It works by finding the K data points in a training dataset that are most like a new data point, using a distance metric to calculate the distance between data points. Then, for classification, it assigns the new data point the label of the most frequent class among its K nearest neighbors, while for regression, it predicts the average value of the target variable (Rahman et al., 2023) and (Cover & Hart, 1967). KNN is an instance-based and non-parametric learning method that performs well with small datasets, although computational demands may increase as the dataset size grows.

KNN is a non-parametric method that does not make any assumptions about the underlying distribution of the data. This makes it a useful tool for working with data that does not follow a known distribution or when the decision boundary between classes is highly irregular. As the acceleration datasets for the railroad bridge under study are extremely non-linear, KNN is found to be one of the suitable classifiers for the detection and classification of damage.

“Closeness” is defined in terms of a distance metric, such as Euclidean distance (Han et al., 2012). The Euclidean distance between two points or tuples, say,  $X_1 = x_{11}, x_{12}, x_{13} \dots x_{1n}$  and  $X_2 = x_{21}, x_{22}, x_{23} \dots x_{2n}$  is,

$$\text{dist}(X_1, X_2) = \sqrt{\sum_{i=1}^n (x_{1i} - x_{2i})^2} \quad (6.10)$$

Typically, the values of each attribute should be normalized before using the above equation (Han et al., 2012).

In this study, the following KNN algorithms under all KNNs classifier are evaluated to classify the damage cases: (i) Fine KNN (ii) Medium KNN (iii) Coarse KNN (iv) Cosine KNN (v) Cubic KNN (vi) Weighted KNN

## 6.2. Damage Classification

In this study, broadly three types of damage are classified including (i) damage in the railroad bridge only (damage to stringer-to-girder joints) and (ii) damage in the rail only, and (iii) combinations of damage to both the bridge and rail. For further classification, they are labeled in three categories as below to see how the difference between these damage cases can be identified through ML classifiers.

The MATLAB application "Classification Learner" was used to classify the type and extent of damage on the railroad bridge under the moving load of Amtrak Acela train described in chapter IV. The railroad bridge under study (Devon railroad bridge) was subjected to different speeds of the train ranging from 15 m/s to 70 m/s, and the induced acceleration signals recorded by sensors attached to various joints without considering noise. Two machine learning

classifiers, namely SVM and KNN were employed to classify damage labels (MATLAB R2022a). The aim was to determine which machine learning algorithm (i.e., SVM and KNN) would yield the highest classification accuracy for the dataset and how much. A total of 1296 data points consisted for this data analysis and a five-fold cross-validation ( $k=5$ ) technique was used to train the classifiers. Here, the dataset is divided into 5 equal-sized subsets, and the model is trained and evaluated 5 times, each time using a different subset for validation. Cross-validation helps to prevent overfitting, which occurs when a model performs well on the training data but poorly on new data. By evaluating the model on multiple validation sets, cross-validation provides a more accurate estimate of how the model will perform on new data. All the datasets (100%) are used to train the classification learner so the new datasets need to be arranged and fed for testing by the classifier.

### **6.2.1. Damage in the Bridge Deck without Rail Defect**

In this case, the damage to the stringer-to-girder (StG) has been considered in different labels such as high damage, low damage, and no damage (healthy case) but the rail in the bridge has no damage (not broken). The results and accuracy of classification from two different classifiers are discussed below.

Various characteristics present in the dataset were extracted through different features associated with three different types of damage labels: Healthy Rail Healthy Bridge (HRHB), Healthy Rail Low Damaged Bridge (HRLDB) and Healthy Rail High Damaged Bridge (HRHDB).

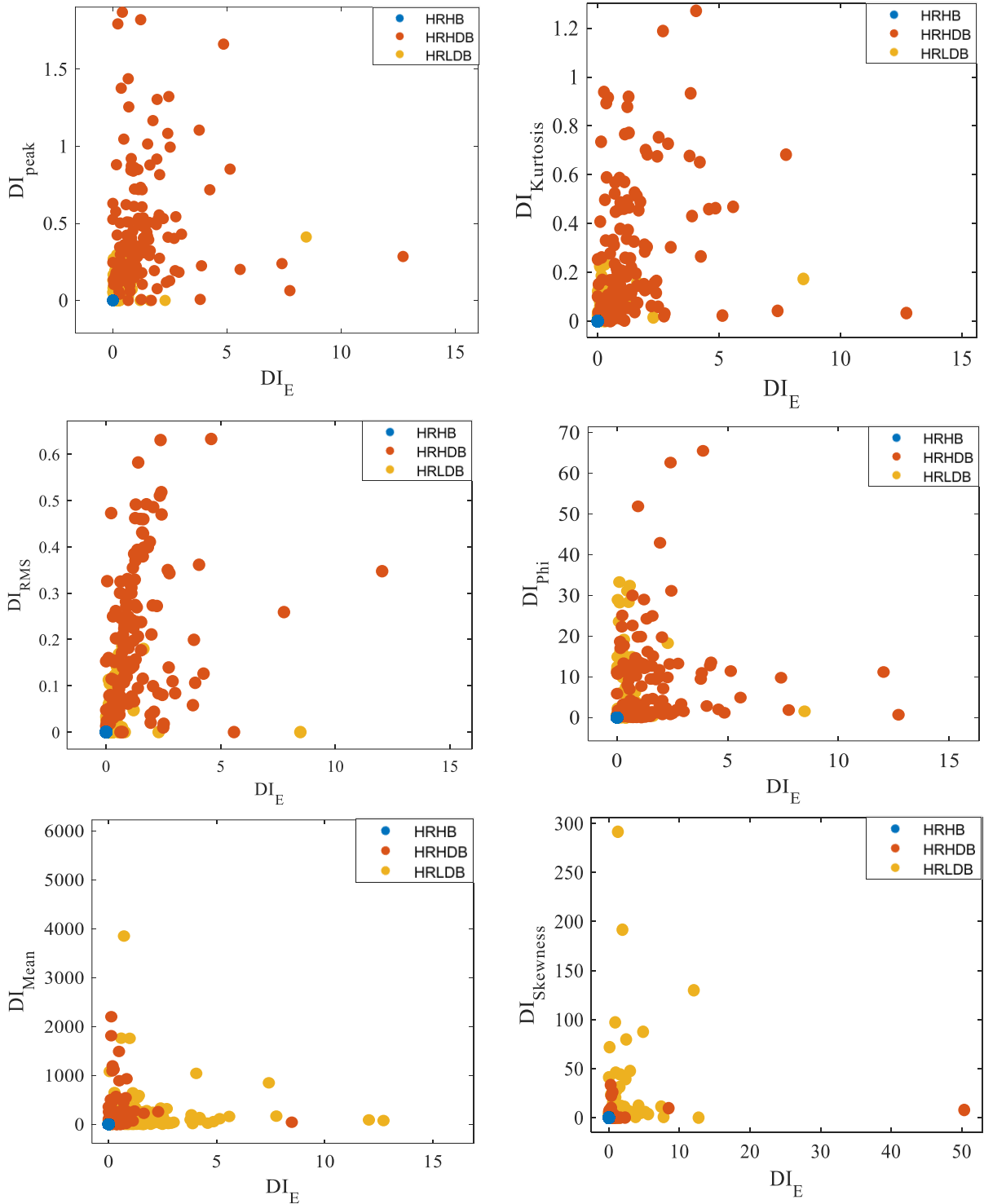


Figure 6. 2 Scatter plot of Energy vs different features (Healthy Rail)

Figure 6.2 shows the scatter plots of  $DI_E$  (energy) versus other features represented by  $DI_i$ , where i is Peak, Kurtosis, RMS, Phase, mean and skewness. In these figures, the blue circle

represents the healthy case where  $(DI_E, DI_i)=(0,0)$ , the yellow circles represent HRLDB case, and the red circles represent HRHDB case. It is seen that the damage indices corresponding to features: kurtosis, peak, and RMS have a better representation of damage to the StG compared to those corresponding to phase, mean, and skewness.

Figure 6.3 displays the confusion matrices for both SVM and KNN algorithms for healthy rail case, which illustrate the evaluation metrics used to assess these machine learning classifiers. Similarly, Table 6.1 summarizes the accuracy validation, precision, sensitivity, and F1-value for each classifier. Among all the algorithms included, the SVM algorithm with a Fine Gaussian kernel achieved the highest accuracy of 95.1% in identifying various types of damage cases from the dataset. The Medium Gaussian SVM utilizes a Gaussian kernel which results in a more precise decision boundary, leading to better classification performance. It also outperformed the other classifier in terms of precision, sensitivity, and F1 value. A higher sensitivity score from SVM indicates that it can correctly identify actual positive cases. The confusion matrix for SVM indicates that approximately 410 data points were predicted with true positive and negative ratings.

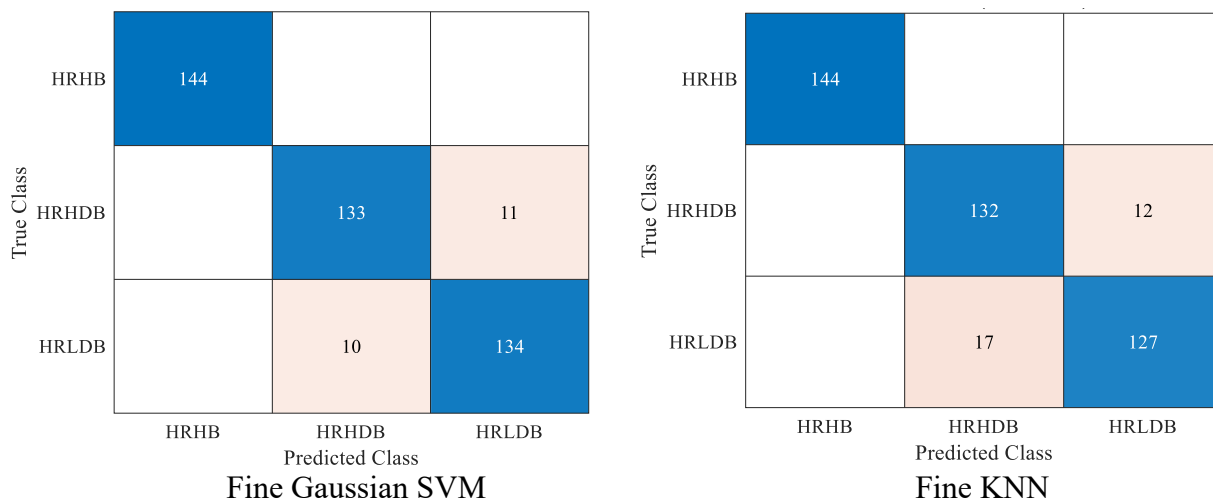


Figure 6. 3 Confusion matrix for SVM and KNN algorithms

Table 6. 1 Evaluation metrics for ML classifiers used in the data-analytic study.

ML Classifier	Accuracy Validation	Precision	Recall	F1 Value
		$\frac{TP}{(TP + FP)}$	$\frac{TP}{(TP + FN)}$	$2 \times \frac{Precision \times Recall}{Precision + Recall}$
SVM- (Fine Gaussian SVM)	95.1%	95.14%	95.14%	95.14%
K-Nearest Neighbors (Fine KNN)	93.3%	93.3%	93.32%	93.31%

The following shows the details of calculation of Precision, Recall and F1-values for confusion matrix (SVM):

- TP: For column 1, the number of HRHB damage case classified correctly =144, for column 2, the number of HRHDB damage case classified correctly = 126 and for column 3, the number of HRLDB damage case classified correctly = 140.
- FP: For column 1, HRLDB falsely classified as HRHB = 1, for column 2, HRLDB falsely classified as HRHDB= 3 and for column 3, HRHDB falsely classified as HRLDB = 18
- FN: For row 1, number of cases classified as Not HRHB = 0, for row 2, number of cases classified as Not HRHDB = 18 and for row 3, number of cases classified as Not HRLDB = 1+3

Therefore, for Overall Precision we can conclude that: Precision for column 1 =  $144 / (144+0) = 100\%$ , Precision for column 2 =  $133 / (133+10) = 93.0\%$ , Precision for column 3 =  $134 / (134+11) = 92.41\%$ , and Overall precision = Average of precision of all columns = 95.14%.

Similarly, for Overall Recall, we can calculate Recall for row 1 =  $144 / (144+0) = 100\%$ , Recall for row 2 =  $133 / (133+11) = 92.36\%$ , Recall for row 3 =  $134 / (134+10) = 93.05\%$ , and Overall Recall = Average of Recall of all rows =  $95.14\%$ , Then F1-value =  $95.14\%$

### 6.2.2. Damage in the Bridge Deck with Rail Defect

Similarly, the damage to the stringer-to-girder (StG) has been considered in different labels such as high damage, low damage, and no damage (healthy case) and at the same time the rail section in the bridge also has damage (broken rail) with reduced E as mentioned in chapter V. The results and accuracy of the classifiers are shown below.

The characteristics in the dataset were extracted through different features associated with following different types of damage labels: Damaged Rail Healthy Bridge (DRHB), Damaged Rail Low Damaged Bridge (DRLDB) and Damaged Rail High Damaged Bridge (DRHDB).

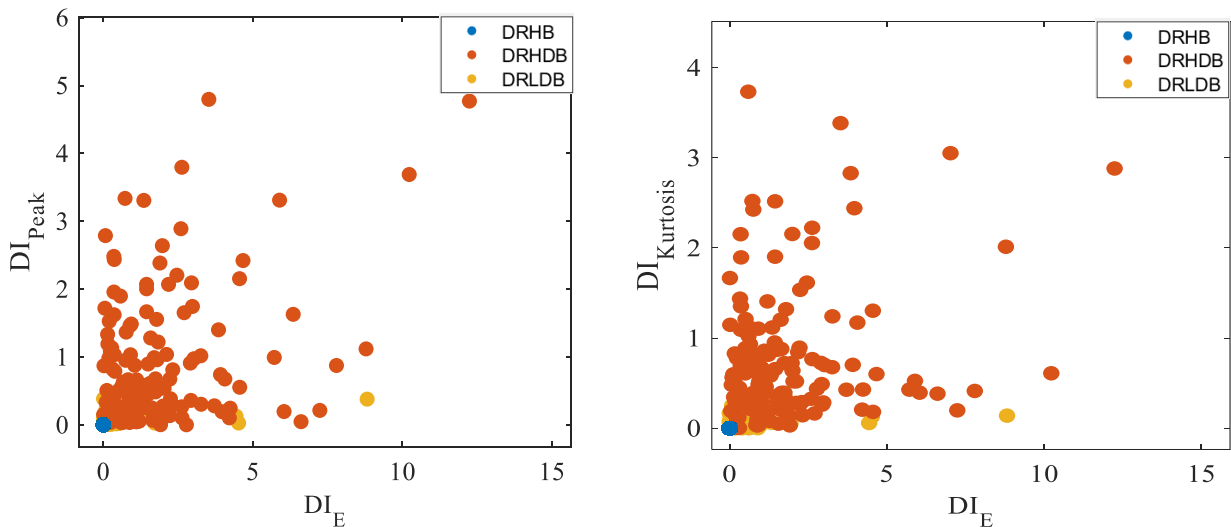


Figure 6. 4 Scatter plot of Energy vs different features (Damaged Rail)

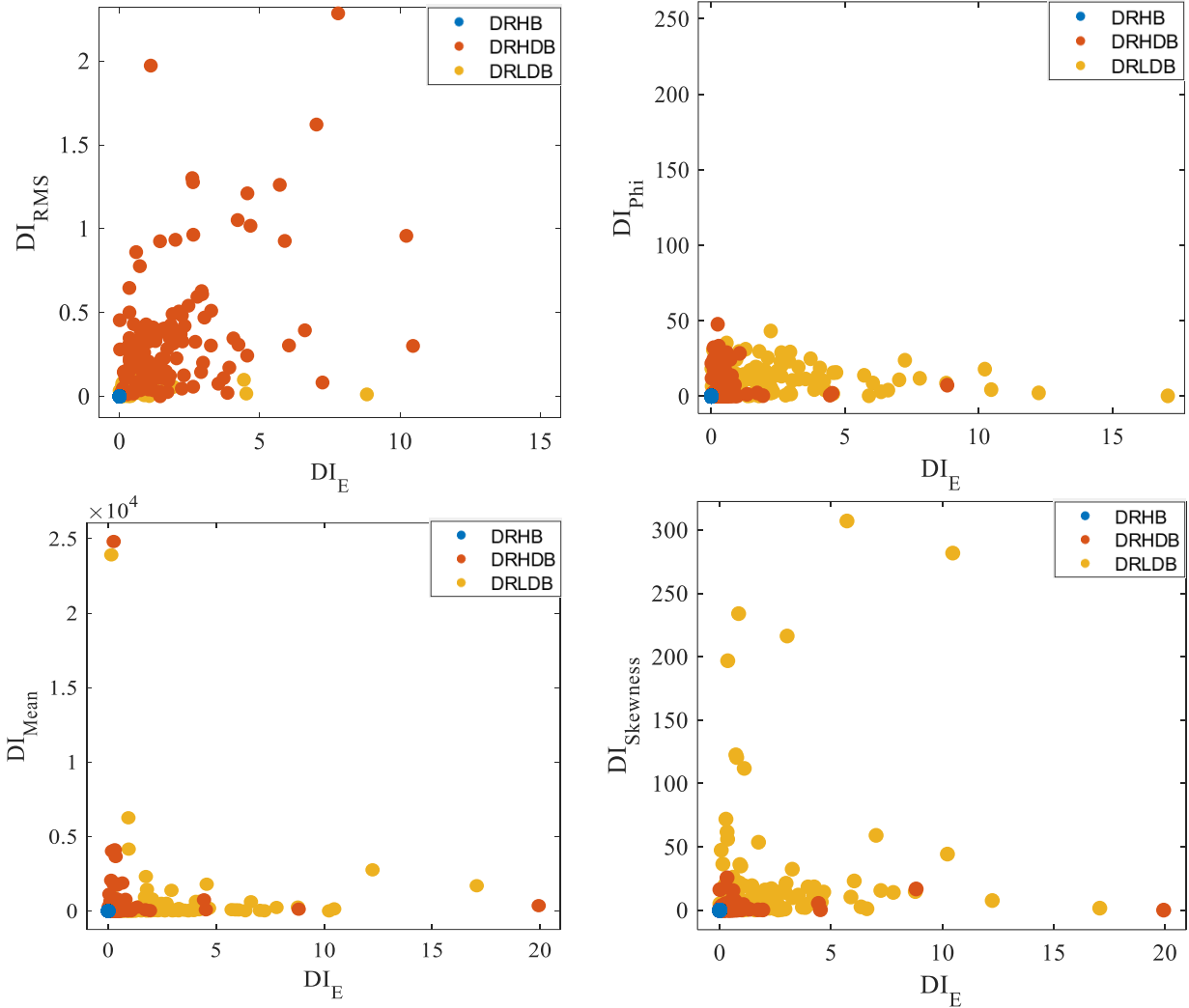


Figure 6. 4, contd.

Figure 6.4 shows the scatter plots of  $DI_E$  (energy) versus other features represented by  $DI_i$ , where  $i$  is Peak, Kurtosis, RMS, Phase, mean and skewness. In these figures, the blue circle represents the healthy case where  $(DI_E, DI_i)=(0,0)$ , the yellow circles represent DRLDB case, and the red circles represent DRHDB case. It is seen that the damage indices corresponding to features: kurtosis, peak, and RMS have a better representation of damage to the StG compared to those corresponding to phase, mean, and skewness.

Figure 6.5 displays the confusion matrices for both SVM and KNN algorithms for damaged rail cases, which illustrate the evaluation metrics used to assess these machine learning

classifiers. Similarly, Table 6.2 summarizes the accuracy validation, precision, sensitivity, and F1 value for each classifier. Among the algorithms, the SVM algorithm with a Linear SVM achieved the highest accuracy of 98.1% in identifying various types of damage cases from the dataset. The Cubic SVM results in a more precise decision boundary, leading to better classification performance. It also outperformed the other classifier in terms of precision, sensitivity, and F1 value. A higher sensitivity score from SVM indicates that it can correctly identify actual positive cases. The confusion matrix for SVM indicates that approximately 415 data points were predicted with true positive and negative ratings.

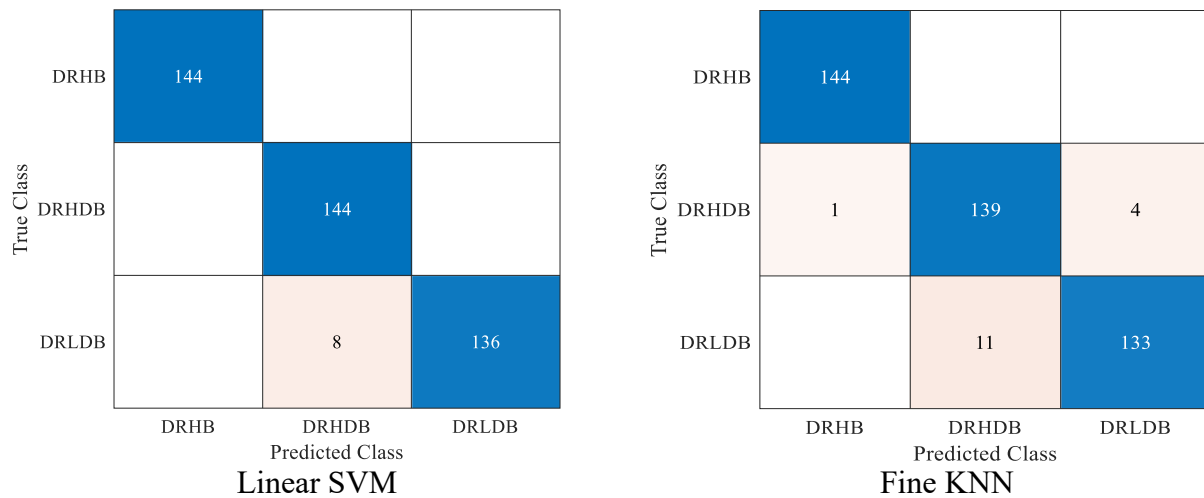


Figure 6. 5 Confusion matrix for SVM and KNN algorithms (Rail defect)

Table 6. 2 Evaluation metrics for ML classifiers used in the data-analytic study.

ML Classifier	Accuracy Validation	Precision	Recall	F1 Value
		$\frac{TP}{(TP + FP)}$	$\frac{TP}{(TP + FN)}$	$2 \times \frac{Precision \times Recall}{Precision + Recall}$
SVM- (Cubic SVM)	98.1%	98.13%	98.25%	98.19%
K-Nearest Neighbors (Fine KNN)	96.3%	92.36%	96.35%	94.31%

### 6.2.3. Combination of damages in Bridge and Rail

In this section, it is intended to identify and classify the rail defect from the healthy rail and damaged rail vibration signals. The machine learning classifiers can detect the defect in the rail and damage in the StG through the acceleration signal.

The characteristics in the dataset were extracted through different features associated with following different types of damage labels: Healthy Rail Healthy Bridge (HRHB), Damaged Rail Healthy Bridge (DRHB) and Healthy Rail High Damaged Bridge (HRHDB).

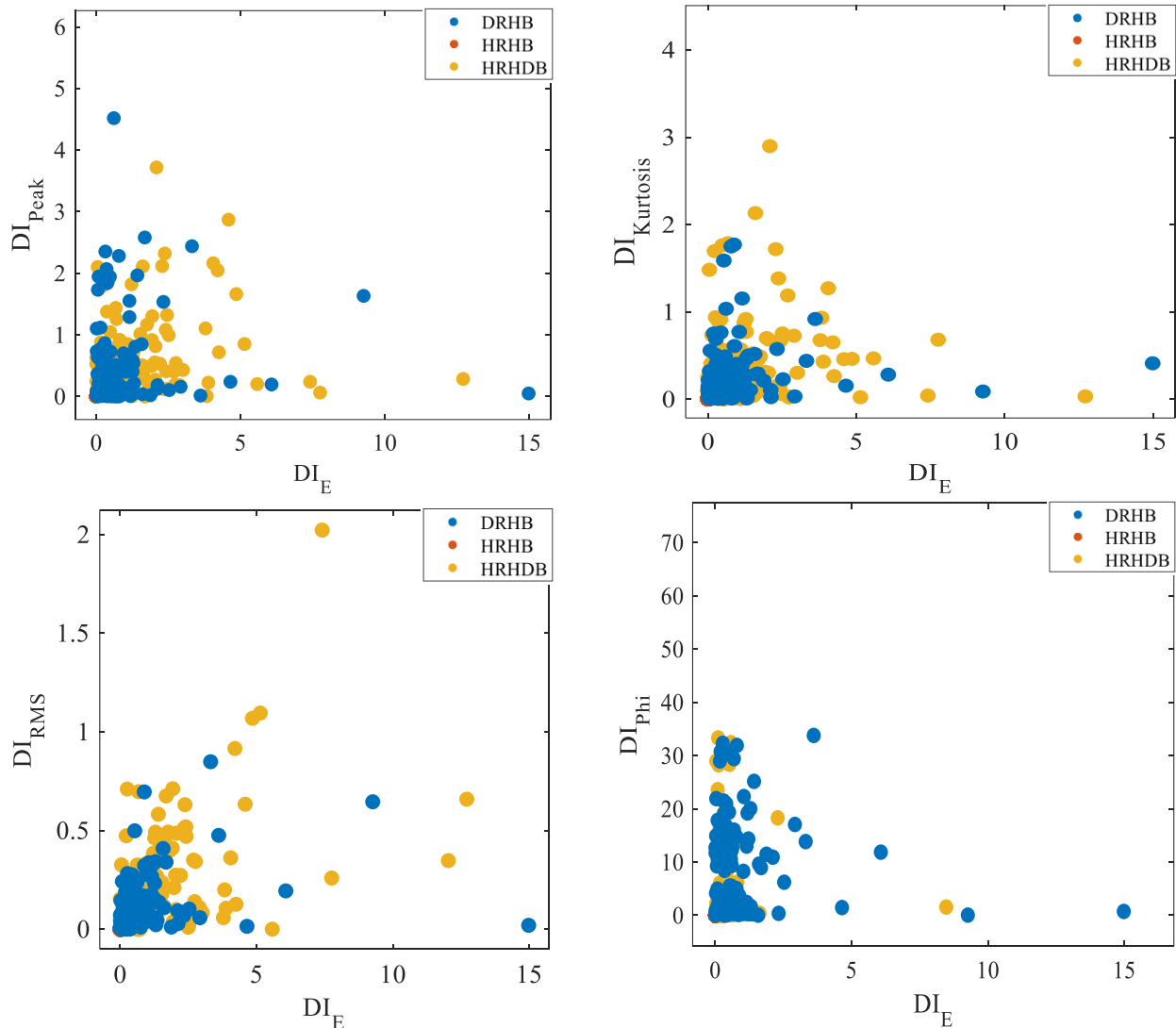


Figure 6. 6 Scatter plot of Energy vs different features (Damaged vs Undamaged Rail & Bridge)

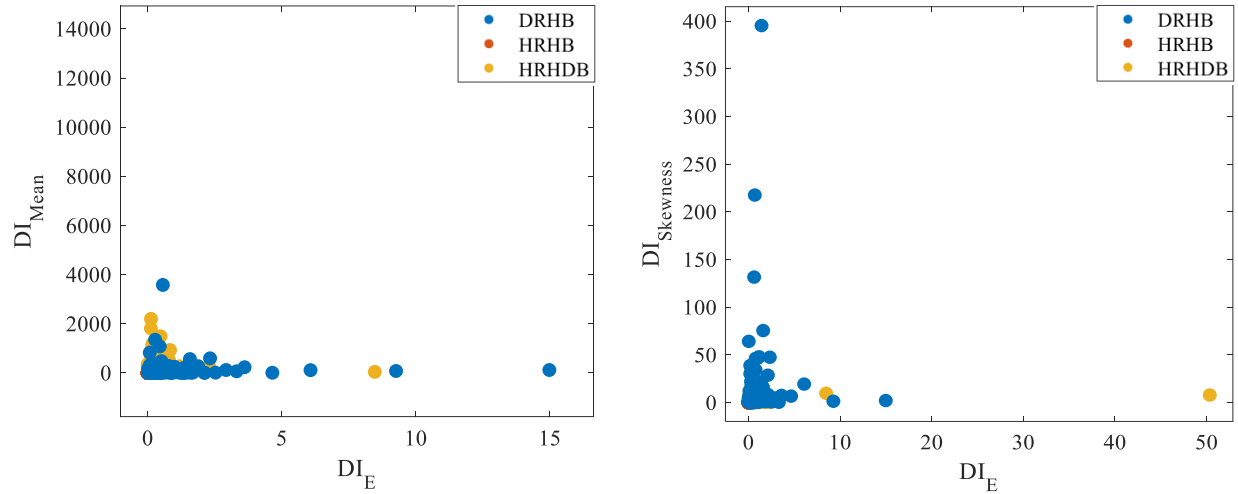


Figure 6. 6, contd.

Figure 6.6 shows the scatter plots of  $DI_E$  (energy) versus other features represented by  $DI_i$ , where  $i$  is Peak, Kurtosis, RMS, Phase, mean and skewness. In these figures, the red circle represents the healthy rail and healthy bridge case where  $(DI_E, DI_i) = (0, 0)$ , the blue circles represent DRHB case, and the yellow circles represent HRHDB case. It is seen that the damage indices corresponding to features: kurtosis, peak, and RMS have a better representation of damage to the StG compared to those corresponding to phase, mean, and skewness.

Figure 6.7 displays the confusion matrices for both SVM and KNN algorithms for combination of damaged and undamaged rail and bridge cases, which illustrate the evaluation metrics used to assess these machine learning classifiers. Similarly, Table 6.3 summarizes the accuracy validation, precision, sensitivity, and F1 values for each classifier. Among the algorithms, the SVM algorithm with a Fine Gaussian SVM achieved the highest accuracy of 87.5% in identifying rail damage from the dataset. The Fine Gaussian SVM results in a more precise decision boundary, leading to better classification performance. It also outperformed the other classifier in terms of precision, sensitivity, and F1 value. A higher sensitivity score from SVM indicates that it can correctly identify actual positive cases. The confusion matrix for SVM

indicates that approximately 390 data points were predicted with true positive and negative ratings.

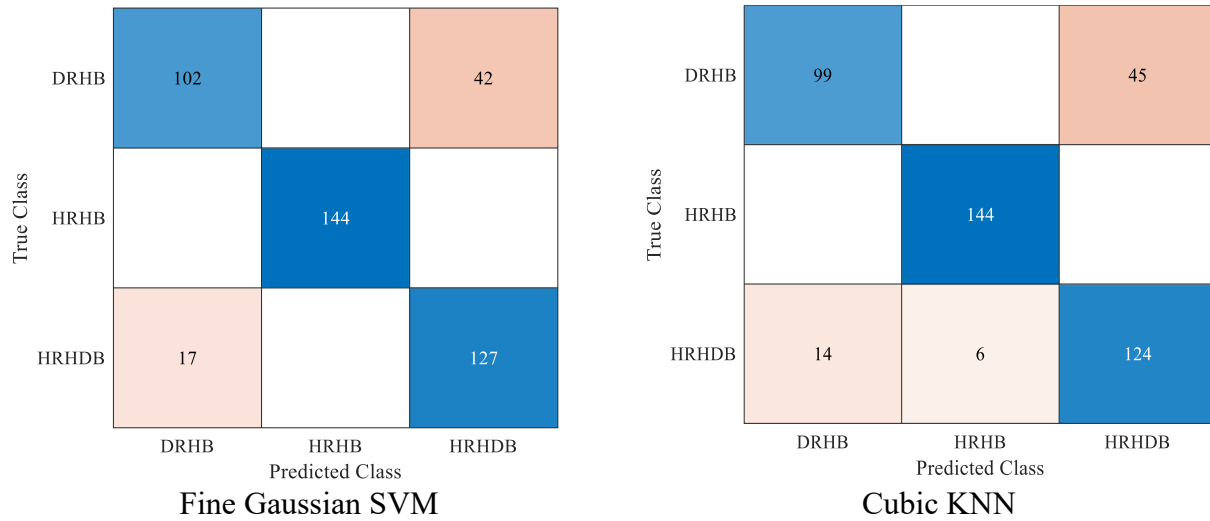


Figure 6. 7 Confusion matrix for SVM and KNN algorithms (Damaged vs Undamaged Rail)

Table 6. 3 Evaluation metrics for ML classifiers used in the data-analytic study.

ML Classifier	Accuracy Validation	Precision	Recall	F1 Value
		$\frac{TP}{(TP + FP)}$	$\frac{TP}{(TP + FN)}$	$2 \times \frac{Precision \times Recall}{Precision + Recall}$
SVM- (Fine Gaussian SVM)	87.5%	86.34%	86.95%	86.64%
K-Nearest Neighbors (Cubic KNN)	85.0%	84.95%	85.67%	85.31%

## CHAPTER VII

### CONCLUSIONS

An open deck steel truss railroad bridge was modeled in 3D finite element software SAP 2000 to identify and predict damage in the rail and bridge structure. Dynamic analysis was performed to generate acceleration responses from the sensors installed at different location of the bridge. Three different damage cases were investigated considering change in rotational stiffness of the Stringer-to-Girder (StG) joint at the mid panel of the bridge. Different time domain features (from Statistical features) and time-frequency domain features (from Hilbert-Huang Transform) in terms of damage indices (DI) were obtained from the acceleration response of healthy and damaged rail and bridge cases. The datasets (DIs) were extracted at corresponding damage labels of Healthy Rail with Healthy Bridge (HRHB), Healthy Rail with Damaged Bridge (HRDB) and Damaged Rail with Damaged Bridge (DRDB). Two different Machine Learning classifiers, Support Vector Machine (SVM) and K-Nearest Neighbor (KNN) were used for classification of the datasets. After analyzing the results of the machine learning classifiers utilized in this research for all three cases, it can be inferred that,

- The SVM algorithm is significantly more effective at classifying and detecting the undamaged and damaged rail and bridge components based on the dataset from dynamic analysis of FE model.

- The accuracy of the classification of the damaged and undamaged bridge either with rail defect or no defect in rail is more than 95%. Similarly, the accuracy of the identification of rail defect in the bridge was more than 85%.

## REFERENCES

- Arvidsson, T., & Karoumi, R. (2014). Train–bridge interaction – a review and discussion of key model parameters. *International Journal of Rail Transportation*, 2(3), 147–186. <https://doi.org/10.1080/23248378.2014.897790>
- Avci, O., Abdeljaber, O., Kiranyaz, S., Hussein, M., Gabbouj, M., & Inman, D. J. (2021). A review of vibration-based damage detection in civil structures: From traditional methods to Machine Learning and Deep Learning applications. In *Mechanical Systems and Signal Processing* (Vol. 147). Academic Press. <https://doi.org/10.1016/j.ymssp.2020.107077>
- Azim, M. R., & Gül, M. (2021). Development of a Novel Damage Detection Framework for Truss Railway Bridges Using Operational Acceleration and Strain Response. *Vibration*, 4(2), 422–443. <https://doi.org/10.3390/vibration4020028>
- B. Svendsen et al (2020) Damage detection applied to a full scale steel truss bridge. (n.d.).
- Baniya, S. B., Baniya, S., Major Advisor, B., Malla, R. B., Advisor, A., Christenson, R., & Kim, J. (n.d.-a). Modeling and Analysis of a Steel Truss Railroad Bridge Traversed by Trains at Various Speeds Masters of Science Thesis Modeling and Analysis of a Steel Truss Railroad Bridge Traversed by Trains at Various Speeds.
- Baniya, S. B., Baniya, S., Major Advisor, B., Malla, R. B., Advisor, A., Christenson, R., & Kim, J. (n.d.-b). Modeling and Analysis of a Steel Truss Railroad Bridge Traversed by Trains at Various Speeds Masters of Science Thesis Modeling and Analysis of a Steel Truss Railroad Bridge Traversed by Trains at Various Speeds.
- Björklund, L. (n.d.). Preface.
- Chalouhi, E. K., Gonzalez, I., Gentile, C., & Karoumi, R. (2017). Damage detection in railway bridges using Machine Learning: Application to a historic structure. *Procedia Engineering*, 199, 1931–1936. <https://doi.org/10.1016/j.proeng.2017.09.287>
- Chen, D. L., Liu, J. X., Du, K. J., & Wang, Y. (2014). Analysis of the deterioration of harmonic local irregularity on locomotive wheel-rail vertical force. *Applied Mechanics and Materials*, 684, 137–144. <https://doi.org/10.4028/www.scientific.net/AMM.684.137>
- Cover, T. M., & Hart, P. E. (1967). Nearest Neighbor Pattern Classification. *IEEE Transactions on Information Theory*, 13(1), 21–27. <https://doi.org/10.1109/TIT.1967.1053964>

- Foster, C. D., & Kulkarni, S. (2021). Coupled Multibody and Finite Element Modelling of Track Settlement. *Lecture Notes in Civil Engineering*, 126, 258–265. [https://doi.org/10.1007/978-3-030-64518-2\\_31](https://doi.org/10.1007/978-3-030-64518-2_31)
- Gao, Y., Wang, P., Wang, K., Xu, J., & Dong, Z. (2021). Damage tolerance of fractured rails on continuous welded rail track for high-speed railways. *Railway Engineering Science*, 29(1), 59–73. <https://doi.org/10.1007/s40534-020-00226-7>
- Han, J., Kamber, M., & Pei, J. (2012). Classification. In *Data Mining* (pp. 393–442). Elsevier. <https://doi.org/10.1016/B978-0-12-381479-1.00009-5>
- Hou, R., Jeong, S., Lynch, J. P., Ettouney, M. M., & Law, K. H. (2022). Data-driven analytical load rating method of bridges using integrated bridge structural response and weigh-in-motion truck data. *Mechanical Systems and Signal Processing*, 163. <https://doi.org/10.1016/j.ymsp.2021.108128>
- Huang, N. E., & Wu, Z. (2008). A review on Hilbert-Huang transform: Method and its applications to geophysical studies. <https://doi.org/10.1029/2007RG000228>
- Kara, O. E. (2011). FIELD TESTING AND FINITE ELEMENT ANALYSIS FOR EVALUATION OF RAILROAD BRIDGES.
- Karoumi, R. (n.d.). Response of Cable-Stayed and Suspension Bridges to Moving Vehicles Analysis methods and practical modeling techniques.
- Kim, R. E., & Spencer, B. F. (2015). NSEL Report Series Modeling and Monitoring of the Dynamic Response of Railroad Bridges using Wireless Smart Sensors. <http://www.terrageria.com/>
- Lei, Y. (2016). Intelligent fault diagnosis and remaining useful life prediction of rotating machinery. Butterworth-Heinemann.
- Lindamood, B., Richards, D. R., Sumner, S., Riehl, W., Niemeyer, P., Thatcher, D., McCarthy, P. O., W Lochner, P. H., Berry, R. G., Burlington Northern Santa Fe Railway, P., McLeod, J., Eng, P., Riley, J. E., Brown, C. J., Hntb, P., & Chambers, C. (n.d.). A R E M A C O M M I T T E E 2 4-E D U C A T I O N & T R A I N I N G Railway Structures.
- Lou, P. (2007). Finite element analysis for train-track-bridge interaction system. *Archive of Applied Mechanics*, 77(10), 707–728. <https://doi.org/10.1007/s00419-007-0122-4>
- Malekjafarian, A., Golpayegani, F., Moloney, C., & Clarke, S. (2019). A machine learning approach to bridge-damage detection using responses measured on a passing vehicle. *Sensors (Switzerland)*, 19(18). <https://doi.org/10.3390/s19184035>
- Malekloo, A., Ozer, E., AlHamaydeh, M., & Girolami, M. (2021). Machine learning and structural health monitoring overview with emerging technology and high-dimensional data source

- highlights. In *Structural Health Monitoring*. SAGE Publications Ltd. <https://doi.org/10.1177/14759217211036880>
- Malla, R. B., Jacobs, D., & Suvash Dhakal Surendra Baniya, P. (2017). Rail Safety IDEA Program Dynamic Impact Factors on Existing Long Span Truss Railroad Bridges Final Report for Rail Safety IDEA Project 25. [www.trb.org/idea](http://www.trb.org/idea)
- Mao, L., & Lu, Y. (2013). Critical Speed and Resonance Criteria of Railway Bridge Response to Moving Trains. *Journal of Bridge Engineering*, 18(2), 131–141. [https://doi.org/10.1061/\(asce\)be.1943-5592.0000336](https://doi.org/10.1061/(asce)be.1943-5592.0000336)
- Mehrjoo, M., Khaji, N., Moharrami, H., & Bahreininejad, A. (2008). Damage detection of truss bridge joints using Artificial Neural Networks. *Expert Systems with Applications*, 35(3), 1122–1131. <https://doi.org/10.1016/j.eswa.2007.08.008>
- Montenegro, P. A., Carvalho, H., Ribeiro, D., Caçada, R., Tokunaga, M., Tanabe, M., & Zhai, W. M. (2021). Assessment of train running safety on bridges: A literature review. In *Engineering Structures* (Vol. 241). Elsevier Ltd. <https://doi.org/10.1016/j.engstruct.2021.112425>
- Mousavi, A. A., Zhang, C., Masri, S. F., & Gholipour, G. (2022). Structural damage detection method based on the complete ensemble empirical mode decomposition with adaptive noise: a model steel truss bridge case study. *Structural Health Monitoring*, 21(3), 887–912. <https://doi.org/10.1177/14759217211013535>
- Neves, A. C. (n.d.). *Structural Health Monitoring of Bridges: Data-based damage detection method using Machine Learning*.
- R\_2021-ARTBA-Bridge-Report USA. (n.d.).
- Rageh, A. (n.d.). RIVETED STEEL RAILWAY BRIDGE HEALTH MONITORING AND RIVETED STEEL RAILWAY BRIDGE HEALTH MONITORING AND DAMAGE DETECTION DAMAGE DETECTION. <https://digitalcommons.unl.edu/civilengdiss/155>
- Rageh, A., Eftekhar Azam, S., & Linzell, D. G. (2020). Steel railway bridge fatigue damage detection using numerical models and machine learning: Mitigating influence of modeling uncertainty. *International Journal of Fatigue*, 134. <https://doi.org/10.1016/j.ijfatigue.2019.105458>
- Rahman, M., Amjadian, M., Pokhrel, M., & Tarawneh, C. (n.d.). Machine learning technique for damage detection of rails on steel railroad bridges subjected to moving train load.
- Rojas, A., & Nandi, A. K. (2006). Practical scheme for fast detection and classification of rolling-element bearing faults using support vector machines. *Mechanical Systems and Signal Processing*, 20(7), 1523–1536. <https://doi.org/10.1016/j.ymsp.2005.05.002>

- Roveri, N., & Carcaterra, A. (2012). Damage detection in structures under traveling loads by Hilbert-Huang transform. *Mechanical Systems and Signal Processing*, 28, 128–144. <https://doi.org/10.1016/j.ymsp.2011.06.018>
- Singh, D., & Singh, B. (2020). Investigating the impact of data normalization on classification performance. *Applied Soft Computing*, 97. <https://doi.org/10.1016/j.asoc.2019.105524>
- Sorgenfrei, D. F., & Marianos, W. N. (2000). General • Open Deck • Ballast Deck • Direct Fixation • Deck Details Geometric Considerations • Proportioning • Bridge Design Loads • Load Combinations • Serviceability Considerations 23.1 Introduction 23.1.1 Railroad Network.
- Structural Health Monitoring using Modern Sensor Technology-Long-term Monitoring of the New Årsta Railway Bridge Merit Enckell. (2006).
- Ticona Melo, L. R., Malveiro, J., Ribeiro, D., Calçada, R., & Bittencourt, T. (2020). Dynamic analysis of the train-bridge system considering the non-linear behaviour of the track-deck interface. *Engineering Structures*, 220. <https://doi.org/10.1016/j.engstruct.2020.110980>
- Ticona Melo, L. R., Ribeiro, D., Calçada, R., & Bittencourt, T. N. (2020). Validation of a vertical train–track–bridge dynamic interaction model based on limited experimental data. *Structure and Infrastructure Engineering*, 16(1), 181–201. <https://doi.org/10.1080/15732479.2019.1605394>
- TxDOT. (2019). Texas Rail Plan Chapters.
- Wiberg, J. (n.d.). Railway bridge response to passing trains Measurements and FE model updating.
- Yang, Y. B., Lin, C. L., Yau, J. D., & Chang, D. W. (2004). Mechanism of resonance and cancellation for train-induced vibrations on bridges with elastic bearings. *Journal of Sound and Vibration*, 269(1–2), 345–360. [https://doi.org/10.1016/S0022-460X\(03\)00123-8](https://doi.org/10.1016/S0022-460X(03)00123-8)
- Zhao, J., & Zhang, L. (2012). Structural Damage Identification Based on the Modal Data Change. *International Journal of Engineering and Manufacturing*, 2(4), 59–66. <https://doi.org/10.5815/ijem.2012.04.08>
- Zhongquan, Z., Enochsson, O., Guojing, H., & Elfgren, L. (2009). Finite element analysis of small span reinforced concrete trough railway bridge. *Key Engineering Materials*, 400–402, 645–650. <https://doi.org/10.4028/www.scientific.net/kem.400-402.645>

## APPENDIX

## APPENDIX

### MATLAB CODE FOR ANALYTICAL SOLUTION OF EQUATION (3.10) FOR MAXIMUM MIDPOINT DISPLACEMENT

```
%%% ### Analytical method to solve displacement equation in simply supported bridge  
subjected to a moving load
```

```
clc
```

```
clear
```

```
L=34; % length of simple beam in m
```

```
n=500;% number of nodes
```

```
x=L/2; % Point of beam where deflection is analysed
```

```
v=68.1; % velocity of the train in m/s
```

```
P=-347000; % Weight of the force, N
```

```
m=11400; % [kg/m] Linear density
```

```
EI=9.92e10; % Modulus of Rigidity[Nm2]
```

```
dt = 0.005;
```

```
t=0:dt:L/v; % Range of t for the response
```

```
nt=length(t) ;
```

```
u=zeros(1,nt) ; % Displacement vector
```

```
for i=1:n
```

```
    wi=(i*pi/L)^2*sqrt(EI/m);
```

```

Si=i*pi*v/(wi*L);
    ohmi=Si*wi;
    A=2*P*L^3/(EI*pi^4);
    B=1/(i^4)*sin(i*pi*x/L);
    C=sin(ohmi*t)-Si*sin(wi*t);
    D=(1-Si^2);
    ui=A*B*C/D;
    u=u+ui;

```

```
end
```

```
umax=max(abs(u))*1000;
```

```
figure(1)
```

```
hold on;
```

```
plot(t,u*1000)
```

```
xlabel('time (sec)');
```

```
ylabel('displacement (mm)');
```

## BIOGRAPHICAL SKETCH

MAHESH POKHREL, a presidential research fellowship (PRF) awardee, received his Master of Science degree in Civil Engineering from The University of Texas Rio Grande Valley, Edinburg, Texas in July 2023. Mahesh has got “Outstanding Student Award” for his academic excellence at UTRGV. He worked as a presidential Research Fellow at UTRGV, Texas from Fall 2021 to Summer I 2023. Previously, he worked for United Nations Children’s Fund (UNICEF), Nepal in the capacity of Recovery Engineer (Construction Manager) from June 2018 to August 2021 and National Specialist – Infrastructure and School Safety at World Vision International, Nepal from June 2016 to June 2018. He can be reached at [maheshpokhrel81@gmail.com](mailto:maheshpokhrel81@gmail.com).